Heavy-liquid separation and photo-oxidation kinetic study of soot and graphitic carbon

Marie-Hélène Veilleux

A Thesis

in

The Department

of

Chemistry and Biochemistry

Presented in Partial Fulfillment of the Requirements
for the Degree of Master of Science (Chemistry) at
Concordia University
Montreal, Quebec, Canada

September 2008

Your file Votre référence
ISBN: 978-0-494-45350-6
Our file Notre référence
ISBN: 978-0-494-45350-6

ABSTRACT

Heavy-liquid separation and photo-oxidation kinetic study of soot and graphitic carbon

Marie-Hélène Veilleux

Black carbon (BC) is a highly refractory class of compounds produced by biomass burning and metamorphism of sedimentary rocks. It comprises a continuum of compounds ranging from char and coal, which partly retain the structure of the original source fuel, to soot and petrogenic graphitic carbon, which are products formed through condensation in the gas phase and during metamorphism, respectively. Soot and graphitic carbon, on which this project focuses, are carbon-rich polyaromatic structures with particularly long environmental lifetimes, potentially making them significant contributors to the slowly-cycling carbon cycle. However, recent environmental mass balance studies suggest that soot and graphitic carbon might be more reactive than previously thought. The main focus of this project is to assess the oxidizability of soot and graphitic carbon in natural environments. Sequential long-term UV and ozone exposure experiments of *n*-hexane soot, graphite and residual graphitic carbon isolated from sediment resulted in carbon losses of 27.1, 5.3 and 79.2 %, respectively, suggesting ozonolysis-driven degradation of these samples. In parallel, a micro-scale heavy-liquid fractionation method using sodium polytungstate was developed to separate soot and graphitic carbon in natural samples. This method shows promising results with recoveries >95 % for *n*-hexane soot and graphite, and could therefore allow further studies on the reactivity of each phase separately. Our results emphasize the importance

of reassessing the long-term preservation potential of the slowly-cycling carbon pool through studies on the oxidation mechanisms involved in their degradation.

Acknowledgement

This project could not have been achieved without the help from my supervisor, Yves Gélinas, whom I want to thank for his precious advises and support. I also want to thank my colleagues and my friends for coping with me during those few years, as well as to my parents for their unconditional support at the most needed moments.

Table of content

List of figures

List of tables

The central theme of my current research focuses on organic matter in all natural environments. Organic matter is a fundamental constituent of the biosphere and the most important chemical source of reducing power that fuels all biogeochemical processes on Earth. We are trying to understand the factors that control the formation, composition, and preservation of organic matter, which is central to comprehending the global geochemical cycles of life forming elements, the controls on atmospheric CO_2 concentrations, the generation of atmospheric O_2, and to elucidating the history of life on Earth.

1. Introduction

Black carbon (BC) compounds are derived from the incomplete combustion of fossil fuels and biomass matter as well as by chemical alteration of plant detritus through different metamorphic processes. The macromolecular and highly aromatic structures of the BC materials such as soot and graphitic carbon make them very resistant to natural decomposition processes. Soot and graphitic carbon are thus assumed to be transported almost conservatively to the ocean by land erosion, river and wind transport, where they are deposited on the seafloor. These BC compounds then become incorporated into marine sediments, which constitute the major long-term sink for organic carbon on the Earth.

In this work, sediments were treated to isolate their soot and graphitic carbon components, which were then oxidized using UV radiation and ozone in order to mimic the type of oxidation occurring in natural environments. Oxidation kinetics were

determined using Elemental Analysis (EA), Fourier-Transform Infrared spectroscopy (FTIR) and Differential Thermogravimetric Analysis (DTA). Soot and graphitic carbon present in the isolate were also physically separated by heavy-liquid sedimentation to enable the quantification of their relative contribution to total carbon in the isolate. The recovery of each phase was confirmed by Elemental Analysis-Isotope Ratio Monitoring Mass Spectrometry (EA-IRMS).

1.1 Biogeochemistry

The field of biogeochemistry is a branch of science that integrates complementary aspects of biology, geology and chemistry. Integration of the different perspectives of the three sciences takes place through the interactions occurring between different elements of the Earth system: the biosphere, lithosphere, atmosphere and hydrosphere. The added contribution of these sciences allows a better understanding of the natural processes occurring on Earth.

1.2 The global carbon cycle

The global carbon cycle (Figure 1) is a major biogeochemical process by which carbon circulates through different living and non-living compartments of the Earth. Its main driving forces include an array of geological, biological and chemical reactions and transport mechanisms. The global carbon cycle is highly dynamic and comprises many operationally-defined and interconnected sub-cycles such as the geological and the biophysical carbon cycles. Although the two cycles are inherently interrelated, the geological carbon cycle occurs on a timescale of millions of years (Sundquist & Visser,

2004), whereas the biophysical carbon cycle has a timescale varying between days and thousands of years.

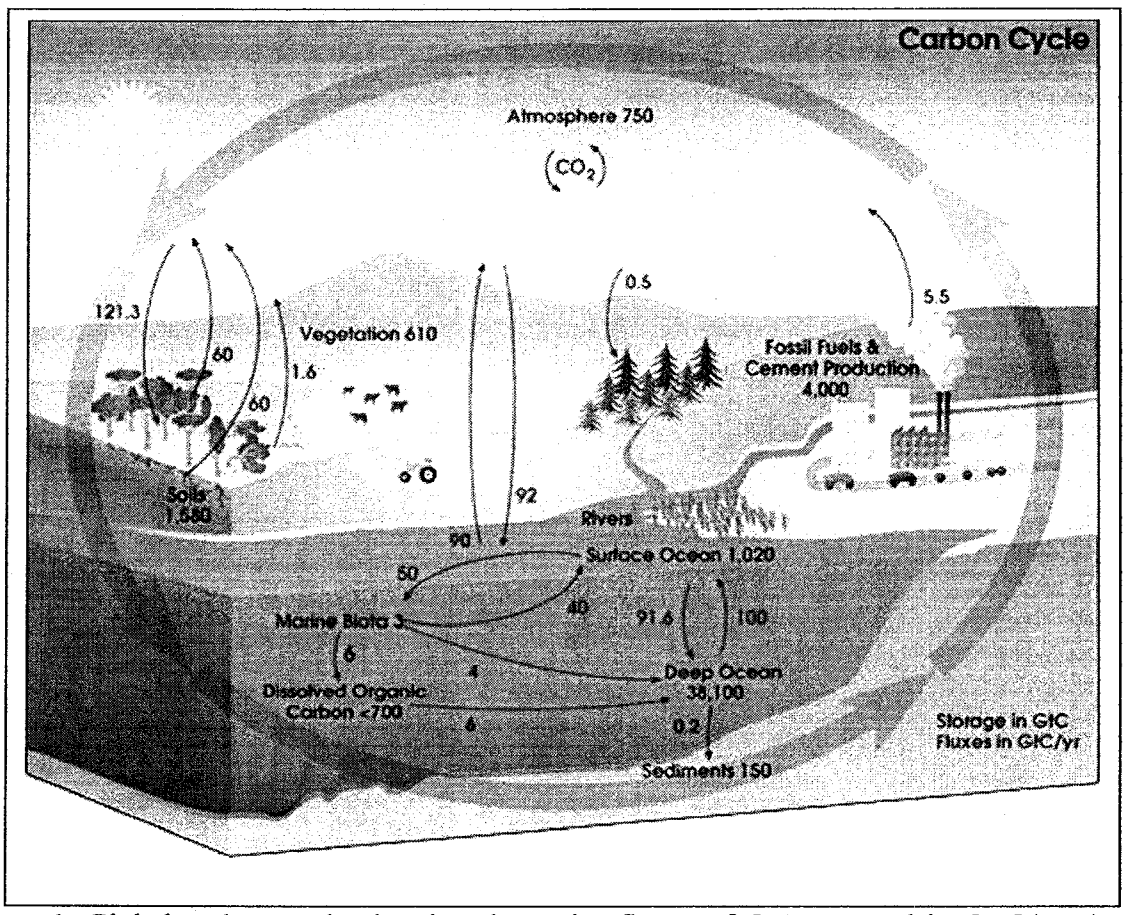

Figure 1. Global carbon cycle showing the major fluxes of C (expressed in Gt C/year) between the different pools (Gt C)

(Ref: http://www.nasa.gov/centers/langley/news/researchernews/rn_carboncycle.html)

1.2.1 The geological carbon cycle

The geological carbon cycle, also called the long-term carbon cycle, involves the exchange of carbon between rocks and the different compartments of the surface of the Earth (ocean, atmosphere, biosphere and soil) over timescales of millions of years. It is

also the most important regulator of the concentration of atmospheric carbon dioxide and oxygen over geological timescales (Berner, 2003; Garrels et al., 1976; Holland, 1978). The interactions between the surface and sub-surface sections happen through different geochemical processes such as uplift and sedimentation, while alteration of carbon bearing components is mostly mediated by metamorphism. A summary of these processes can be represented by the following generalized reaction:

(1) $CO_{2(g)} + CaSiO_{3(s)}$ (or $MgSiO_{3(s)}$) $\rightleftharpoons$ $CaCO_{3(s)}$ (or $MgCO_{3(s)}$) + $SiO_{2(s)}$

This reaction is a simplified representation of the uptake of atmospheric carbon dioxide during the weathering on land of calcium and magnesium silicates present in rocks and minerals to produce solid calcium and magnesium carbonates as well as quartz. Weathering is the physical and chemical alteration of rocks and minerals on the surface of the Earth. Most of the weathered rocks are discharged into the ocean through river transport with an estimated carbon flux of about 1 Gt C yr^{-1} (Suchet et al., 2003) (Gt = 10^{12} kg) for minerals and rocks, including approximately 0.43 Gt C yr^{-1} of terrestrial organic carbon (Schlunz & Schneider, 2000). Physical weathering breaks down rocks and minerals into smaller parts through processes such as abrasion, thermal insolation and slaking. Chemical weathering, on the other hand, involves chemical reactions such as hydrolysis, oxidation, reduction and carbonation between rocks and their immediate environment. An example of chemical weathering of rocks is the hydrolysis of albite, with the input of atmospheric CO_2 in order to produce the hydroxylated form of albite, as seen in the following reaction:

(2) $2NaAlSi_3O_{8(s)} + 2CO_{2(g)} + 11H_2O_{(l)} \rightarrow Al_2Si_2O_5(OH)_{4(s)} + 2HCO^-_{3(aq)} + 2Na^+_{(aq)} + 4H_4SiO_{4(aq)}$

albite

Minerals, rocks, and soils (including their organic carbon fraction), as well as the remains of living organisms, are weathered and transported into the ocean where they are subjected to further chemical and biological transformations before being deposited onto the oceanic floor and buried in sediments. The remaining organic carbon and their inorganic matrices are then transported into the mantle of the Earth by subduction where they are chemically and physically altered by different geological processes. Although marine sediments represent the only long-term carbon pool present on the planet with a residence time of approximately 10,000 to 20,000 years (Forbes et al., 2006), the tectonic plates slowly move the carbon back to the Earth's atmosphere, oceans and crust by volcanic eruptions, hydrothermal vent emissions and orogeny, respectively, thus creating a full geological carbon cycle. The Earth's mantle and crust constitute the most important carbon pool with a carbon storage of about $0.92\text{-}1.6 \times 10^{11}$ Gt C (Mackenzie et al., 2004; Wood et al., 1996). Figure 2 below is a schematic representation of the geological carbon cycle, showing the major carbon fluxes between different geological compartments of the Earth.

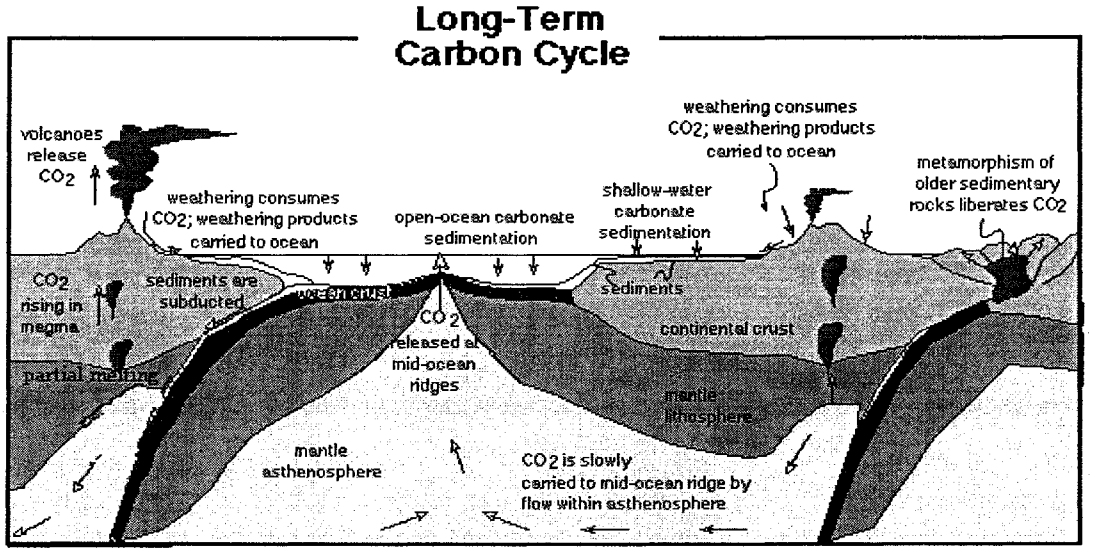

Figure 2. Summary of carbon fluxes in the geological carbon cycle

(Ref: www.carleton.edu/departments/geol/DaveSTELLA/Carbon/long_term_carbon.htm)

Metamorphism is a geological process by which minerals and rocks entering the Earth by burial or subduction are physically and chemically altered under high heat and pressure. This process starts at a temperature of about 100-150 °C up to about 900 °C and involves pressures up to 13,000 Atm. The transformation of minerals and rocks undergoing metamorphism mainly involves dehydration and recrystallization. Most types of metamorphism end with the return of modified minerals and rocks to the surface of the Earth by processes such as orogeny (i.e., the process of natural mountain building). While metamorphism mainly alters carbon in its inorganic form, other geological processes transform the organic forms of carbon. For example, coal is formed from the transformation of organic matter present in peat through a maturation process named coalification (see below for a description of its chemical composition). Coal formation, as seen in Figure 3, slightly overlaps metamorphism since its ending phase occurs deep in

the Earth, where temperature and pressure reach high values. The early stages of coalification involve a brief aerobic decay in which the volume of accumulated plant debris on the bottom of a peat is significantly decreased by bacterial activity. This first stage is then followed by anaerobic bacterial decay until the acidity produced by the decay kills the anaerobic bacteria (the pH decreases to about 4). The percentage of carbon is then thermally increased by the release of water, hydrogen and oxygen at a temperature of about 100 °C. There are a number of different parameters used to classify coal into different categories (called "ranks"); these include carbon, hydrogen and oxygen contents, moisture and volatile matter, reflectance and calorific value. Owing to the widely variable nature of coal, no single parameter can be used as a classification tool throughout the entire coal range. A generally accepted classification of the different types of coal based on reflectance and elemental contents is presented in Table 1 below.

Table 1. Classification of coal rank

Rank	Refractive index	OC† (%)	Atomic H/C† (mole ratio)	Atomic O/C† (mole ratio)
Sub-bituminous	0.4 – 0.5	70 – 80	0.75 – 1.00	0.15
High-volatile bituminous	0.6 – 1.1	80 – 90	0.60 – 0.75	0.10
Medium-volatile bituminous	1.1 – 1.5	80 – 90	0.50 – 0.75	0.05 – 0.10
Low-volatile bituminous	1.5 – 1.9	85 – 90	0.50 – 0.75	0.05 – 0.10
Semi-anthracite	2.0	90	0.50	0.05
Anthracite	3.0	> 90	0.25 – 0.50	< 0.05
Meta-anthracite	> 4.0	> 90	0.25	< 0.05

†OC is organic carbon, while H/C and O/C are the molar hydrogen-to-carbon and oxygen-to-carbon ratios, respectively. Ref.: Modified from Orem & Finkelman, 2003.

The formation of graphite occurs at the extreme level of coalification, where metamorphic conditions are reached with temperatures ranging around 300 – 500 °C and pressures of more than 3,000 Atm (Kwiecinska & Petersen, 2004). The rate of coalification is strongly related to temperature, pressure and time. Although most studies agree that formation of coal (from sub-bituminous to anthracite) occurs at temperatures between 100 °C and 275 °C (Daniels et al., 1994; Francis, 1954; Pesek & Sykorova, 2006; Taylor et al., 1998), the pressure required for its formation is still debated as it is

generally agreed that time is a more important variable in the formation of coal products (Pesek & Sykorova, 2006). The present reserves of coal are estimated at between 5,000 – 10,000 Gt C (Houghton, 2003).

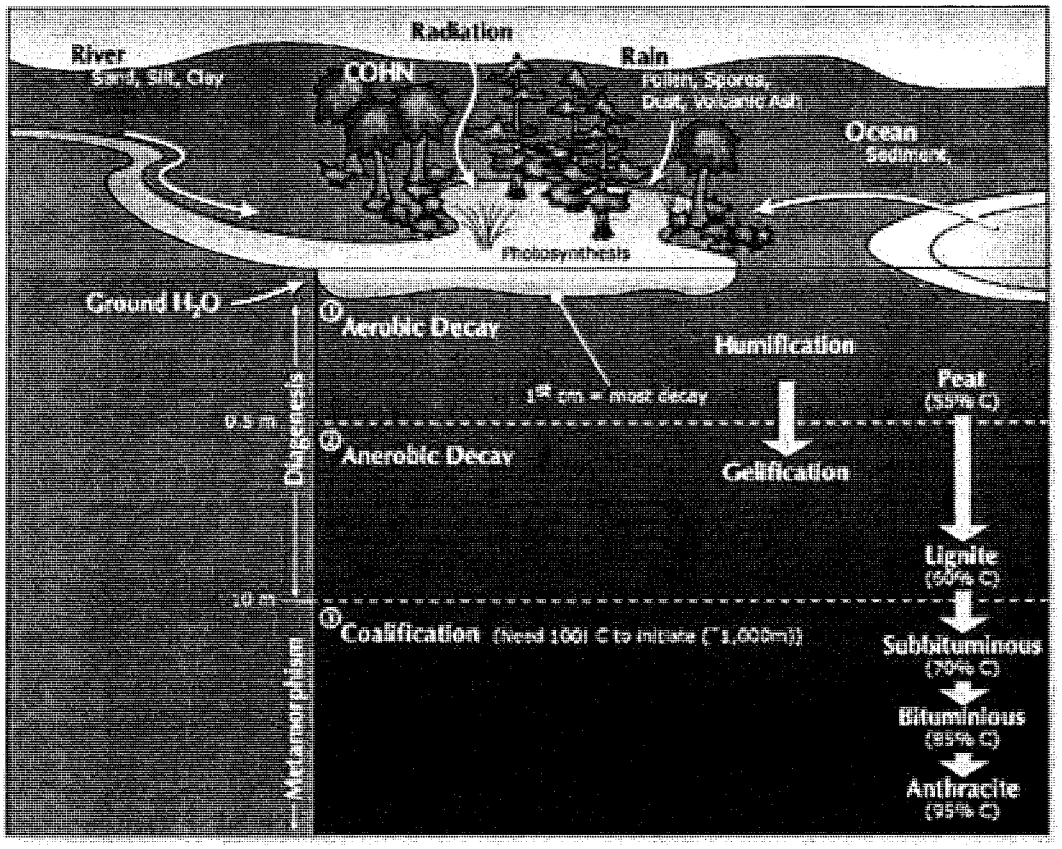

Figure 3. The coalification process, showing the different steps leading to the formation of coal (modified from ref.: http://smtc.uwyo.edu/coal/swamp/anatomy.asp)

The geological carbon cycle is a long-term cycle that encompasses many geological processes involving the transport and alteration of carbon between different carbon reservoirs including the atmosphere, soil, rivers and oceans as well as the Earth's mantle.

The chemical reactions and physical changes involved in the interactions between the different reservoirs are so numerous and occur under such variable conditions that it is very hard to classify each reaction and its products into clearly defined divisions.

1.2.2 The biophysical carbon cycle

While the geological carbon cycle is related mainly to the formation, transformation and transport of carbon-containing minerals and rocks, the biophysical carbon cycle deals mostly with the degradation of organic carbon either transported to or produced within the oceans. Although the two cycles happen in different locations on the Earth as well as on different timescales, they nonetheless remain intimately intertwined through the discharge of minerals and rocks from rivers but also from the burial of organic carbon that is later transformed by metamorphism.

The biophysical carbon cycle relates to the direct interactions between carbon stored in the atmosphere, the ocean and on land. The atmosphere and the oceans are two major reservoirs of carbon with approximately 7.85×10^5 Gt C and 3.85×10^7 Gt C, respectively (Li, 2000; Mackenzie et al., 2004). The direct exchange of carbon dioxide between the atmosphere and the ocean, called the solubility pump, occurs from changes in partial pressure at the air-sea interface as well as from changes in water temperature. An intake in atmospheric CO_2 by the ocean occurs when the partial CO_2 pressure of the ocean is lower than the atmosphere. The carbon flux is estimated at about 90 Gt C yr^{-1} in both directions (Houghton, 2003; Prentice et al., 2001), thus no significant net increase in carbon dioxide is present in any medium. The high solubility of CO_2 in cold water, as

compared to other gases, contributes to the high uptake of this gas into the ocean, where it is found in three forms: dissolved CO_2 (about 0.5 % of total CO_2 forms), HCO_3^- (about 87.5 %) and CO_3^{2-} (about 10.5 %) (Sarmiento, 1993). An uptake of CO_2 by the ocean thus results in a decrease in pH of the ocean water through the formation of dissolved HCO_3^-. The different forms of CO_2 are interrelated through equations (3) and (4), in which, for example, an increase in atmospheric CO_2 results in a higher dissolved CO_2 concentration in seawater, and to in a direct increase in HCO_3^- through the reaction between dissolved CO_2 and the CO_3^{2-} ions already present in the system.

(3) $$CO_{2(g)} + H_2O_{(l)} \rightleftharpoons H_2CO_{3\,(aq)} \rightleftharpoons HCO_3^-{}_{(aq)} + H^+_{(aq)} \rightleftharpoons CO_3^{2-}{}_{(aq)} + 2H^+_{(aq)}$$

(4) $$CO_{2(dissolved)} + CO_3^{2-}{}_{(aq)} + H_2O_{(l)} \rightleftharpoons 2HCO_3^-{}_{(aq)}$$

The decrease in CO_3^{2-} concentration through its reaction with CO_2 limits further uptake of CO_2 by the ocean and thus restricts the buffering capacity of the ocean towards increases in atmospheric CO_2 concentrations.

The biological pump (Figure 4), a process by which atmospheric carbon dioxide is fixed as organic (reduced) carbon in the surface ocean and transferred to the intermediate and deep ocean, also regulates the flow of carbon between the atmosphere and the ocean. Phytoplankton, photosynthetic micro-organisms present at the surface water of oceans, plays a major role in the biological pump by transforming about 120 Gt C $year^{-1}$ of

HCO_3^- into sugars during photosynthesis (Ciais et al., 1997) and releasing about half of this newly incorporated CO_2 through respiration (Lloyd & Farquhar, 1996; Waring et al., 1998). The magnitude of photosynthesis and respiration each year is 1000 times greater than the amount of carbon transported through the geological carbon cycle, thus emphasizing the importance of phytoplankton on the biophysical carbon cycle. The role of phytoplankton in ocean carbon chemistry is even more important as it represents the first level of the marine trophic food chain. The organic matter produced by phytoplankton is either used by other marine fauna in the surface water or sinks out of the photic zone to the deep ocean. This carbon enrichment in the deep ocean also contributes to the reduction of CO_2 at the surface. It is estimated that marine photosynthesis followed by the sinking of organic matter to the deep ocean maintains the atmospheric CO_2 concentration to about 30 % of what it would be in the absence of the biological pump (Houghton, 2003).

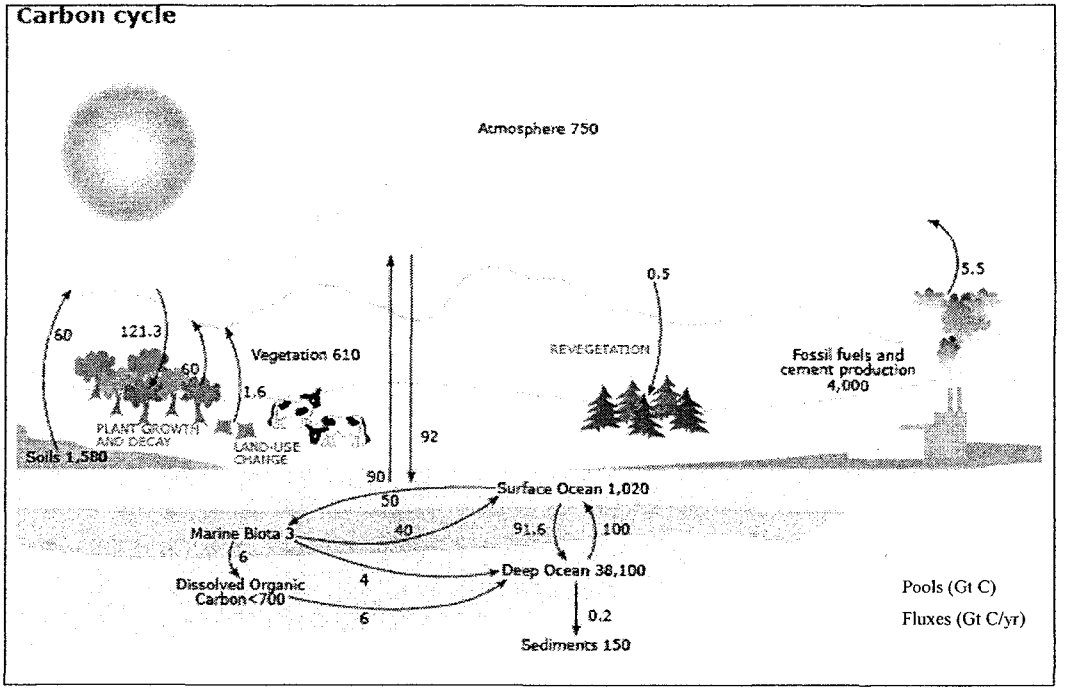

Figure 4. The biophysical carbon cycle showing the main pools (expressed in Gt of C) and fluxes (in Gt C/year) of C. (Ref.: http://www.ozcoasts.org.au/glossary/def_c-d.jsp)

Organic matter present in the surface water is subjected to remineralization processes, including reactions such as hydrolysis and oxidation, which degrade organic matter to carbon dioxide, water and nutrients and thus reduce the flux of particulate organic carbon sinking through the water column. Remineralization of organic matter is more intense in the shallower part of the water column, where sunlight promotes marine life, and decreases with depth such that a very small fraction of organic compounds synthesized in the surface ocean eventually reaches the sediments at the bottom of the ocean. It is estimated that about 99.5 % of marine production and about 50 % of terrestrial organic matter introduced to the ocean is remineralized in the water column, thus resulting in a global flux of total organic carbon to marine sediments of about 0.1 –

0.2 Gt C yr^{-1} (Hedges et al., 1997). Total organic carbon content of marine sediments ranges from < 2.5 mg C g_{dw}^{-1} in open ocean to 200 mg C g_{dw}^{-1} in organic rich coastal and continental margin sediments (Burdige, 2007).

Selective preservation of organic matter also plays an important role in the decrease of labile organic matter through the water column and occurs following three pathways. The first is the enzymatic depolymerization of polysaccharides to oligo- and monomeric sugars which are thought to undergo random abiotic condensation with other substances such as low-molecular-weight lipids to form refractory organic compounds usually referred to as humic substances (Burdige, 2007). The second mechanism involves the production and selective preservation of hydrolysis-resistant, non-labile macromolecules by certain biological organisms present in the ocean, while the third one involves the protection of organic matter through the interaction of labile organic compounds with inorganic matrices (i.e., mineral protection). These mechanisms of preservation either yield macromolecules that are sometimes too large to be chemically characterized using conventional hydrolysis and chromatographic methods, or compounds that cannot be separated from their mineral matrix. In fact, only about 30 – 40 % of the organic carbon in marine particles reaching the surface of the sediments can be characterized by conventional analytical techniques.

1.3 Black carbon and graphitic carbon residue

The molecularly uncharacterized organic carbon buried in marine sediments includes compounds that have traditionally been considered highly refractory to

biological and chemical degradation, such as BC. BC is a generic term that encompasses a continuum of compounds comprising biomass and fossil fuel combustion products as well as products of metamorphism. BC components range from slightly charred, degradable biomass to highly condensed and refractory graphite. The BC continuum contains a range of compounds with increasing carbon content and aromaticity. The physical and chemical properties of a given class of compounds also change with formation pathways. Coal, for example, is a product of metamorphism through its formation by coalification; it retains some of the physical and chemical properties of its source material (peat), while soot, formed from the condensation of hot gases present in flames of combusted solid and liquid fuels, retains only a minute fraction of the physical and chemical properties of its source material. Combustion of biomass and fossil fuel, for which the production of all types of C estimates range from 0.05 to 0.27 Gt C $year^{-1}$ (Druffel, 2004; Kuhlbusch & Crutzen, 1995) and from 0.012 to 0.024 Gt C $year^{-1}$ (Druffel, 2004; Penner et al., 1993) respectively, produces particles in varying sizes that determine their potential atmospheric residence time, with smaller particles such as soot traveling farther and larger particles such as charcoal settling nearby their site of formation. This contrasting behavior enables their use as paleotracers. Since the vast majority of soot particles produced from biomass burning are smaller than 1 μm (Cachier et al., 1995), they can remain suspended in the atmosphere for months (Ogren & Charlson, 1983) and can thus travel long distances before being deposited back on the Earth's surface, either on land or in water bodies. Figure 5 below illustrates the BC continuum:

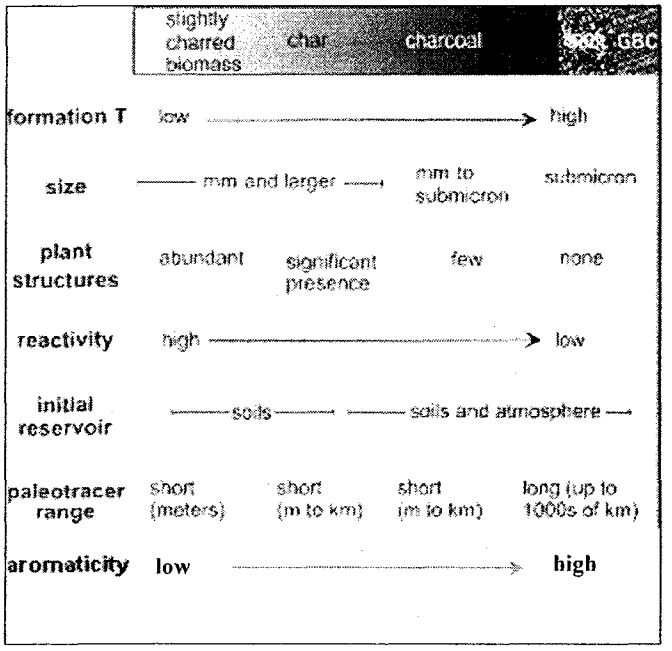

Figure 5. The BC continuum with the major components and relevant characteristics

[†]GBC is graphitic black carbon, which corresponds to the soot and graphitic carbon fraction isolated from natural samples following the method of Gélinas et al., 2001.

(Ref.: Modified from Masiello, 2004)

The macromolecular structure of BC and its high degree of aromaticity makes it highly resistant to biological and chemical degradation in natural environments. While small soot particles can relatively easily be oxidized, graphitic carbon (polyaromatic carbon characterized by structures ranging from amorphous and highly ordered with small defects) and graphite (mostly highly ordered polyaromatic carbon) are especially difficult to degrade due to their highly aromatic macromolecular structures and their lack of oxygen-containing functional groups. Given that BC is continually formed in the modern environment and using the lower end of the estimated BC production rate (0.05

Gt BC $year^{-1}$), calculations based on the historical global production rate of BC from natural and anthropogenic sources, coupled to the estimated global organic carbon sedimentation rate in the world ocean, show that present-day sedimentary organic carbon would be composed of about 30% in BC in the absence of any degradation on the surface of the Earth (details in Kuhlbusch & Crutzen, 1995). Although such high percentage of BC contribution to sedimentary organic carbon has been reported in some abyssal sediments, the vast majority of sediments typically contain organic carbon with a relative contribution of only about 3 – 10 % in BC (Hedges & Keil, 1995), thus suggesting the existence of a non-sedimentary BC sink or a greater degradation potential of the material than currently assumed.

Methodological uncertainties in the measurement of BC concentrations lead to an even greater discrepancy between BC production and loss estimates since there is currently no universal method that can isolate and quantify BC in soil and sediment matrices. Although a number of different methods currently used to isolate the BC continuum have been reported in the literature, most of these are operationally-defined and isolate different portions of the continuum based on the technique they use. The different methods include: microscopic counting of the number of charcoal pieces visible under an optical microscope; removal of thermally oxidizable BC compounds upon heating; removal of chemically labile compounds through chemical extraction; thermochemical extraction of chemically and thermally labile compounds. An intercomparison study on the efficiency of the most commonly used methods for determining BC concentrations resulted in concentrations varying by a magnitude of

more than 500 for the same sample (Masiello, 2004; Schmidt et al., 2001). Discrepancies among the different methods result from the lack of a common definition for BC materials and potential biases due to overestimation caused by condensation reactions occurring when macromolecular biopolymers are depolymerised and volatilized at high temperatures (Maillard, 1912). Failure to detect portions of the BC continuum also results in negative biases.

A new method designed to reduce these potential artefacts through the removal of chemically and thermally labile components of the sample was recently published (Gélinas et al., 2001). The method was designed to isolate the most refractory components of the BC continuum, soot and graphitic carbon, from complex minerals and organic matrices. Although graphitic carbon and graphite have long been assumed totally unoxidizable under natural conditions, they have never been studied separately in terms of their resistance to oxidative degradation. This method, along with a second one aiming at separating soot and graphitic carbon, allowed testing of our working hypothesis that in fact, graphitic carbon and graphite present in natural environments are more labile than previously thought, thus providing a partial explanation for the missing back carbon sink.

1.4 General objectives of the project and organization of the thesis

The main objective of this project was to assess the relative oxidation rates of selected BC compounds including bituminous coal, soot and graphite, in order to test the

hypothesis that graphitic carbon is oxidized by UV radiation and exposure to ozone at natural levels when present at the surface of soil or in rock formations directly exposed to the atmosphere. This was accomplished by exposing BC compounds to UV radiation and ozone for a period of 977 hrs in ambient conditions. Morphologic and molecular changes were monitored during oxidation using EA, FTIR and DTA. A microscale method used to separate soot and graphitic carbon was also developed using density fractionation with the heavy liquid sodium polytungstate. The method was validated using organic carbon and stable carbon isotope mass balances on several separate standards and natural samples.

Chapter 2 lists the materials and methods used in this project and describes the analytical challenges that are associated with the analysis of this type of compounds. In particular, the difficulty to completely thermally oxidize BC compounds during elemental analysis and the low response of BC to FTIR spectroscopy are presented. In Chapter 3, the optimization of the method developed in this work to physically separate soot and graphitic carbon from natural sediments is described, along with the stable carbon isotope signature approach exploited to evaluate separation efficiencies. The results obtained on the oxidation of certain BC compounds by photolysis and ozonolysis are then presented and discussed in Chapter 4. Changes in carbon masses, chemical and thermal lability of BC compounds are explained, along with possible oxidation pathways for soot and graphite.

2. Analytical difficulties associated with the analysis of black carbon compounds

There are many analytical difficulties with the detection, characterization and quantification of BC components owing mainly to their structure. BC components are naturally produced from a wide range of compounds varying in aromaticity, hydrogen saturation and O/C ratio. Their molecular composition and structure vary in a continuous way, which prevents the definition of any clear chemical boundaries between the different classes of materials. The classification of BC components is therefore based on morphological and chemical characteristics that change only slightly from one component to the next. This lack of a clear chemical definition leads to many analytical difficulties when studying BC components, the most important being the absence of analytical methods that target specific components of the BC continuum. All the existing "BC" methods are thus operationally defined and a lot of them are at best semi-quantitative. The discrepancies among the different BC methods was evaluated by Schmidt et al. (2001) who found 500-fold variations or more for the same sample measured with the different techniques. One of the main reasons for the problems faced when analyzing BC components is their highly refractory nature as well as their macromolecular structure, which make them insoluble in any solvents. Insolubility makes their analysis complicated by making them unsuitable to conventional chromatographic analytical techniques that require dissolution of the analyte. Research projects focusing on the study of BC are thus analytically extremely challenging (Masiello, 2004).

Some of the analytical difficulties encountered throughout the course of this project are presented and discussed in this chapter. The major aim of this study was to evaluate the oxidation rate of soot and graphitic carbon under natural environmental conditions. Isolates of soot and graphitic carbon from natural sediment as well as BC standards covering a wide range of lability were thus chemically characterized following UV radiation and ozone treatments to determine the rate of oxidation and the concurrent formation/elimination of functional groups occurring upon oxidation. The analyses performed on the natural samples and standards include measurement of carbon and oxygen content, the identification of functional groups by FTIR and evaluation of thermal stabilities by DTA.

2.1 Materials and methods

2.1.1 Material used

A total of twelve standards and natural samples were used in this work. The five BC standards comprised graphite (Alfa, Ward Hill, MA), bituminous coal (Ward's, Rochester, NY), mesquite charcoal, melanoidin (Karen Hammes, University of Zurich, Switzerland) and lab-made *n*-hexane soot (Akhter et al., 1985). Other types of samples that contain contrasting amounts of BC were also analyzed, namely humic acid (Aldrich), Urban Atmospheric Particulates (SRM 1648) and Buffalo River sediment (SRM 2704) standard reference materials (both purchased from the U.S. National Institute of Standards and Technology, Gaithersburg, MD, USA), as well as natural river, lake and coastal sediments. The river sediment was sampled in the bed of the Stillaguamish River, which drains the slopes of the Cascade Mountains north of Seattle (WA, USA, see

Dickens et al., 2004, for a full description of the sampling site); the lake sediment is a 0 to 15 cm integrated sample that was collected in Lake Washington, downwind from downtown Seattle (WA, USA, Dickens et al., 2004). Finally, the continental margin sediment was sampled near the mouth of the McKenzie River on the Canadian Arctic shelf in December 2003 (CASES over-wintering mission on the R/V Amundsen).

The soot sample used in this work was synthesized from the combustion of *n*-hexane following the method described by Akhter et al. (1985). Briefly, ACS grade *n*-hexane (Fisher Scientific) was combusted in a low and wide glass container placed under a inverted glass funnel covered with aluminum foil to close up the drain of the funnel, and attached at a height of approximately 15 cm from the bench top inside a fume hood. A thin layer of *n*-hexane was poured in the container and was set afire with a match. Upon combustion, *n*-hexane forms soot particles that are convectively transported to the surface of the inverted funnel. Following the combustion of a sufficiently large volume *n*-hexane, soot deposited onto the funnel and aluminum foil was scraped off and transferred to a beaker using acetone, which was left to evaporate overnight.

2.2 Methods

2.2.1 Isolation of graphitic carbon residue from sediments

Graphitic carbon residue, containing soot and graphitic carbon, was isolated from natural samples following a chemothermal method recently developed for soils and aquatic sediments (Gélinas et al., 2001). Briefly, the samples were lyophilized, ground with a mortar and pestle into a fine powder and demineralized by dissolving the

carbonates, salts and sesquioxide coatings in 1 N HCl for 30 min. Silicate minerals were then removed by two successive 12 hr treatments with 1 N HCl and 10 % HF at room temperature. Hydrolyzable organic matter (primarily proteins and carbohydrates) was removed by three successive treatments with O_2-free trifluoroacetic acid (TFA) in order to prevent formation of melanoidin-like material[1] (Allard et al., 1998). Treatments involved two hydrolyses with 2 N TFA carried out at 100 °C for 3 hr as well as two additional ones performed at 100 °C for 18 hr with 4 N and 6 N TFA, respectively. Remaining hydrolyzable organic matter was then removed by treatment with 6 N HCl at 110 °C for 24 hr. The residual non-hydrolyzable, non-soot and non-graphitic organic matter fraction was removed by thermal oxidation at 375 °C for 24 hr in an O_2-saturated environment. This method selectively isolates soot and graphitic carbon with standard deviations in residual soot and graphitic carbon conservatively estimated to be ± 15 % (Gélinas et al., 2001), although part of the soot BC fraction (the smallest soot particles) might get oxidized through the catalytic oxidation in the presence of residual minerals (not removed in the HCl and HF steps) and oxygen at 375 °C (Elmquist et al., 2004).

2.2.2 Photolysis and ozonolysis

The BC samples and the soot and graphitic carbon isolated from natural sediments were oxidized by sequential treatments of photolysis and ozonolysis. The oxidation was performed in two steps. First, approximately 30 – 50 mg of samples were placed in individual open aluminum pans of 8 mm in diameter; they were then subjected to UVA (400-320 nm) and UVB (320-280 nm) rays produced in a photochemical reactor

[1] Melanoidin is composed of polyaromatic and heterocycle-rich molecules formed through condensation reactions during pyrolysis.

(Rayonet, The Southern New England Ultraviolet Company, CT, USA), which also generated ozone at a concentration of 6 ppbv, for 551 hr. Second, the same samples were placed in an UVO-cleaner model 342 (Jelight Company Inc., CA, USA) for an additional 426 hr. The UVO-cleaner generates UV rays in the range 184.9 – 546.1 nm, with an ozone concentration varying between 500 and 1000 ppmv (Jelight Company Inc., personal communication). This setup allowed the determination of the effect of oxidation mediated mostly by UV rays, with an ozone concentration similar to those measured in the lower, non-polluted troposphere (e.g., rural areas); the second step allowed compensating for the slow oxidation kinetics of BC compounds by increasing the concentration of ozone to levels that are much higher than in the environment. Although unproven, it is assumed in this work that the increased oxidation kinetics at high ozone concentration adequately mimics the long-term oxidation of BC compounds at natural ozone abundances.

2.2.3 Elemental composition

The carbon and oxygen content of the samples were measured on a Perkin Elmer elemental analyzer model 2400 Series II (Shelton, CT, USA). The carbon content of the samples were measured by inserting the samples into the combustion chamber, where they were combusted to CO_2, H_2O and NO_x through reaction with O_2 gas and a chromium trioxide catalyst. The NO_x gas was then reduced to N_2 by hot metallic copper and the gases mixed and separated by molecular sieve chromatography before reaching the thermal conductivity detector. The samples were prepared by weighing between 0.5 mg and 15 mg of carbonate-free sample in a 3 × 5 mm tin cup and inserting the folded cup

into a combustion chamber that was swept with a carrier gas (helium). The samples weights were chosen to be approximately 0.15 mg C and 0.5 mg O to get the most accurate and precise results, which corresponds roughly to the middle of the dynamic range of the instrument used in this work for carbon and oxygen, respectively. The standards used for the analyses are acetanilide, with 71.09 %C, 6.71 %H, 10.36 %N and 11.84 %O, and cysteine with 29.99 %C, 5.03 %H, 11.67 %N, 26.69 %S and 26.41 %O (all weight percent, both standards from Perkin Elmer Instruments, Norwalk, CT, USA) for the carbon and oxygen analyses, respectively.

The operating conditions for the analyses of carbon were optimized with combustion and reduction temperatures of 1050 °C and 500 °C, respectively. The combustion column consisted of a quartz tube filled with chromium oxide and silvered cobaltous oxide particles, while the reduction of the combustion gases was done using elemental copper particles. The optimal compromise between a complete combustion and wasting of consumables (mainly the elemental copper particles) corresponded to an oxygen filling time and combustion time of 10 s and 120 s, respectively.

The determination of the oxygen content follows the same procedure except that the sample was pyrolyzed in a column filled with nickelized carbon particles, followed by a reduction column at 500 °C containing elemental copper. The carrier gas for the pyrolysis was a mixture of helium and hydrogen (95:5). The CO_2 produced upon pyrolysis was converted to CO over the platinized carbon reagent contained in the combustion chamber along with the elemental copper. The produced carbon monoxide

and the other gases such as H_2 and N_2 were then separated by gas chromatography and detected using a thermal conductivity detector.

2.2.4 Thermogravimetric/Differential thermal analysis

n-hexane soot, graphite, bituminous coal, as well as the isolated soot and graphitic carbon fraction from a natural sediment were analyzed by thermogravimetry/differential thermal analysis (TG/DTA), at different time points during their oxidation by photolysis and ozonolysis, to determine the thermal oxidizability of the residues. The instrument used was a PL Thermal Science STA 1500 DTA/TGA equipped with a microbalance and a furnace capable of heating up to 1500 °C. Depending on the organic carbon content of the sample to be analyzed, between 4 and 10 mg of finely ground samples were weighed into an open platinum pan while a second pan, kept empty, served as the reference. The samples were analyzed under a stream of air (20 $mL \cdot min^{-1}$) and a temperature ramp of 10 °C/min between 20 °C and 1000 °C.

2.2.5 Heavy-liquid density fractionation of soot and graphite

Fractionation of soot and graphite was done using the heavy-liquid sodium polytungstate adjusted to a density of 1.8 $g \cdot mL^{-1}$ with distilled water. Mixtures of the soot and graphitic standards were sonicated for 30 min in siliconized 1.7-mL eppendorf tubes to ensure homogenization of the samples. The samples were then centrifuged at 12,000 rpm for 15 min and the soot supernatant (density = 1.2 – 1.8 $g \bullet mL^{-1}$) and the graphite precipitate (density = 2.1 – 2.3 $g \bullet mL^{-1}$) were vacuum filtered to obtain the two separate phases. The recovered soot and graphite fractions were then analyzed by

elemental analysis – isotope-ratio monitoring mass spectrometry (EA-IRMS) to evaluate the separation efficiency based on their stable carbon isotope ratios signature. A schematic diagram of the fractionation method used is shown in Figure 6.

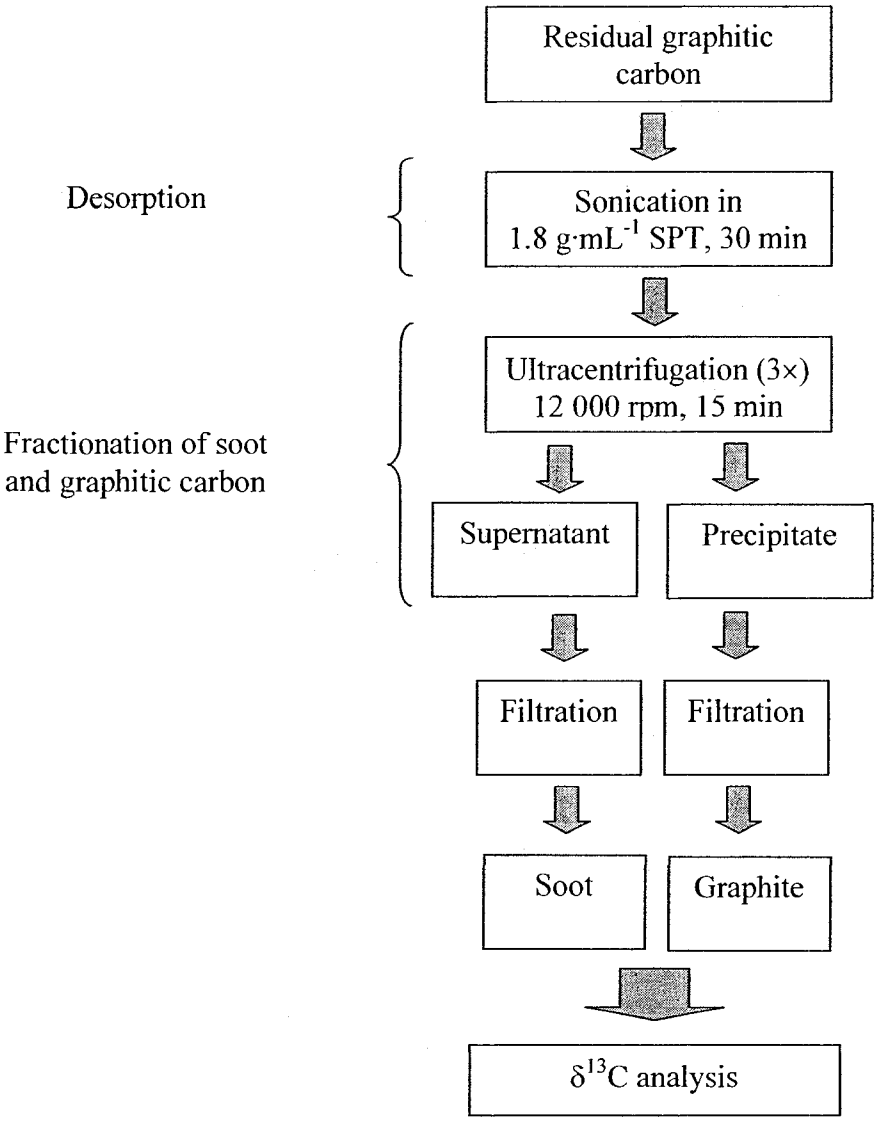

Figure 6. Procedure for the heavy-liquid density fractionation of soot and graphite

The stable carbon isotope signatures were measured on an Eurovector elemental analyzer coupled to a continuous flow isotope-ratio monitoring mass spectrometer (EA-IRMS, Micromass Isoprime, GV Instruments, Manchester, UK). The CO_2, N_2 and H_2O gases produced in the combustion and reduction chambers of the EA (see Section 2.2.3 for details), were passed through a water trap and directed towards a continuous flow inlet allowing the alternative passage of the reference gas and the gases produced from combustion of the sample to the ionization source. The ionized gases were then separated in a magnetic sector mass spectrometer by exploiting the difference in their kinetic energy (owing to their different masses). For the analysis of carbon as CO_2, the ions at masses 44 ($^{12}C^{16}O^{16}O$), 45 ($^{13}C^{16}O^{16}O$ + $^{12}C^{17}O^{16}O$) and 46 ($^{12}C^{18}O^{16}O$ + $^{13}C^{17}O^{16}O$) were directed towards different Faraday cups, as seen in Figure 7.

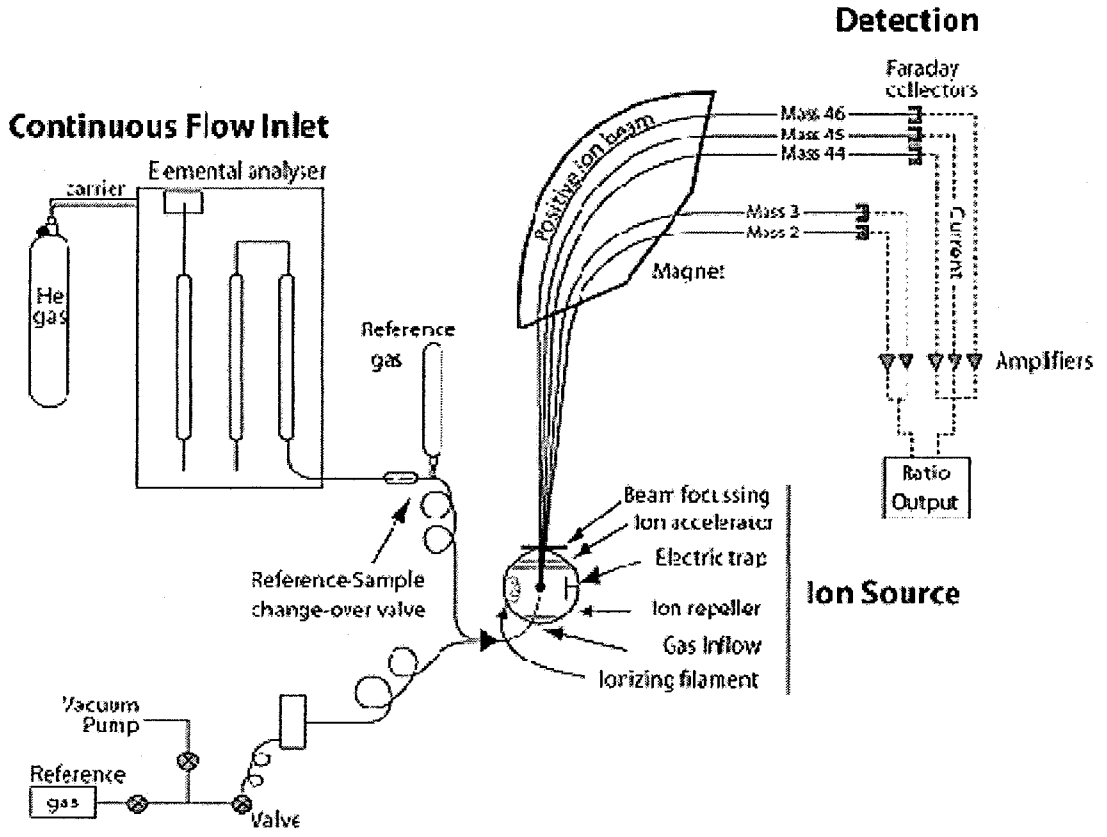

Figure 7. Diagram of an EA-IRMS (Ref. Clark, I. D. and Fritz, P. Environmental Isotopes in Hydrogeology, Lewis Publishers, New York, 1997, p.14)

The ^{13}C isotopic signature, or $\delta^{13}C$, is given as a ratio of the isotopic composition of the sample versus that of a reference CO_2 gas in per mil (‰), as per the following formula:

$$\delta^{13}C_{sample}\ (‰) = [(^{13}C/^{12}C_{sample}) /(^{13}C/^{12}C_{reference} - 1)] \times 1000$$

The efficiency of the separation was then evaluated from the isotope signature of the pure soot and graphite phases (*n*-hexane soot: -24.01 ± 0.30 ‰, graphite: -22.69 ± 0.14 ‰) according to the following formula:

$$\text{percent soot phase (\%)} = \frac{[\delta^{13}C \text{ separated mixture} - \delta^{13}C \text{ pure graphite}]}{[\delta^{13}C \text{ separated graphite} - \delta^{13}C \text{ separated soot}]} \times 100$$

Once the separation efficiency of the fractionation method was proven, separation of soot and graphitic carbon from natural sediments was performed on natural soot/graphitic carbon isolates in order to evaluate the percent composition of each phase in the sediment.

2.2.6 Molecular analyses by Fourier-transform infrared spectroscopy

Fourier-transform infrared (FTIR) spectroscopy was used to qualitatively analyse graphite, *n*-hexane soot, bituminous coal and a graphitic carbon isolate from the Stillaguamish River. Each sample was subjected to 551 hr of ultraviolet radiation followed by 426 hr of elevated ozone exposure. Scans of the non-treated, UV radiated, and UV and ozone exposed samples were performed on a Nicolet 6700 FTIR spectrometer from Thermo Electron Corporation (Waltham, MA, USA) using dry potassium bromide pellets. The compromise between a slow scanning rate and high peak resolution to achieve acceptable signal-to-noise ratios (S/N) on highly absorbing BC samples were thus obtained by purging the window chamber with N_2 for 5 min prior to

each scan and by averaging 256 scans with a resolution of 2 cm^{-1}. The spectral range was 450 – 4000 cm^{-1}.

2.3 Analytical difficulties with elemental analysis

The organic carbon and total oxygen composition of BC samples was measured at several time points during an ozonolysis experiment designed to estimate the oxidation rate of each BC sample (results presented in Chapter 4). As oxidation proceeds with ozone, the samples react to form oxygen-containing functional groups such as ethers, aldehydes and carboxylic acids, which further react to produce volatile organic carbon and CO_2 (see Chapter 4 below for further details). The increase in oxygen-containing functional groups as well as the volatilization of carbon-containing compounds can be monitored by elemental analysis in order to estimate the oxidation rates of the samples. Figure 8 below is a general schematic diagram of an elemental analyzer (carbon detection mode).

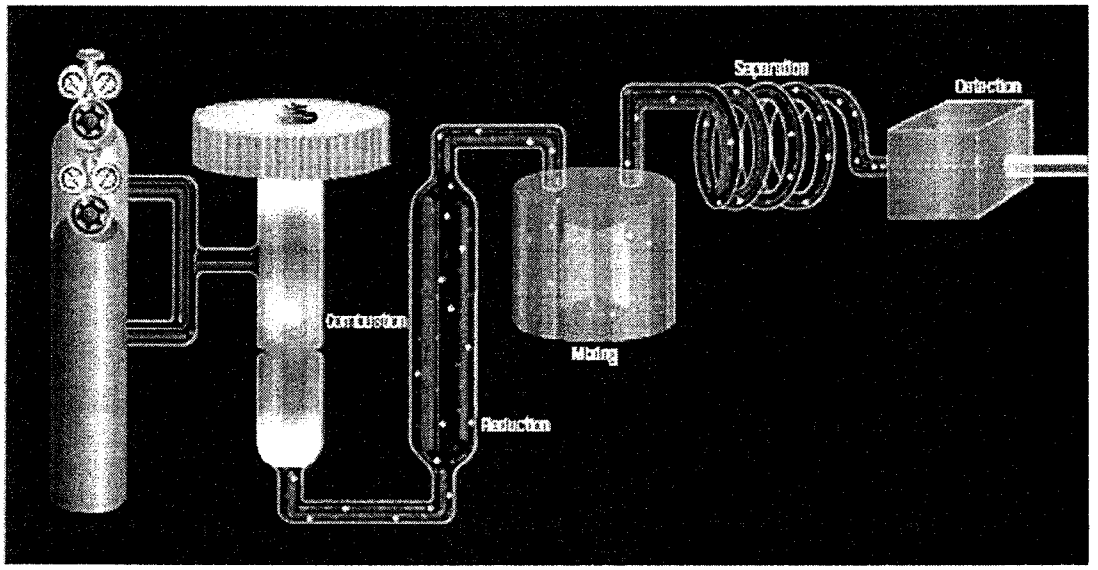

Figure 8. Schematic representation of an elemental analyzer

(Ref: http://las.perkinelmer.com)

While the determination of the elemental composition of organic materials is relatively easy, that of BC compounds and natural sediments can sometimes be problematic. The macromolecular and polyaromatic structure of BC components makes it very hard to thermally oxidize them as a higher relative amount of oxygen and high heat are required to break the carbon-carbon bonds of the structure and form carbon dioxide. Thus, the temperature of the combustion chamber was raised to 1050 °C (the maximum operating temperature) instead of the 975 °C normally used for less refractory samples. The combustion conditions were also optimized by increasing the flow rate of oxygen entering the chamber by 250 % and the combustion time by 400 %, to obtain 615 cc O_2 /s and 120 s, respectively. Although the optimized conditions resulted in a more efficient combustion and in a decrease in memory effects from sample to sample, the most refractory samples were still incompletely combusted. For example, the memory

effect for graphite was reduced from 1.3 % to 0.65 % of the integrated signal intensity after optimization of the combustion conditions. Despite optimization of combustion parameters, the kinetics of oxidation of BC material are most likely too slow to achieve complete thermal oxidation. The analysis of the elemental composition of melanoidin, a somewhat labile BC compound, after 197 hr of UV exposure clearly demonstrates this phenomenon, as shown in Figure 9 below.

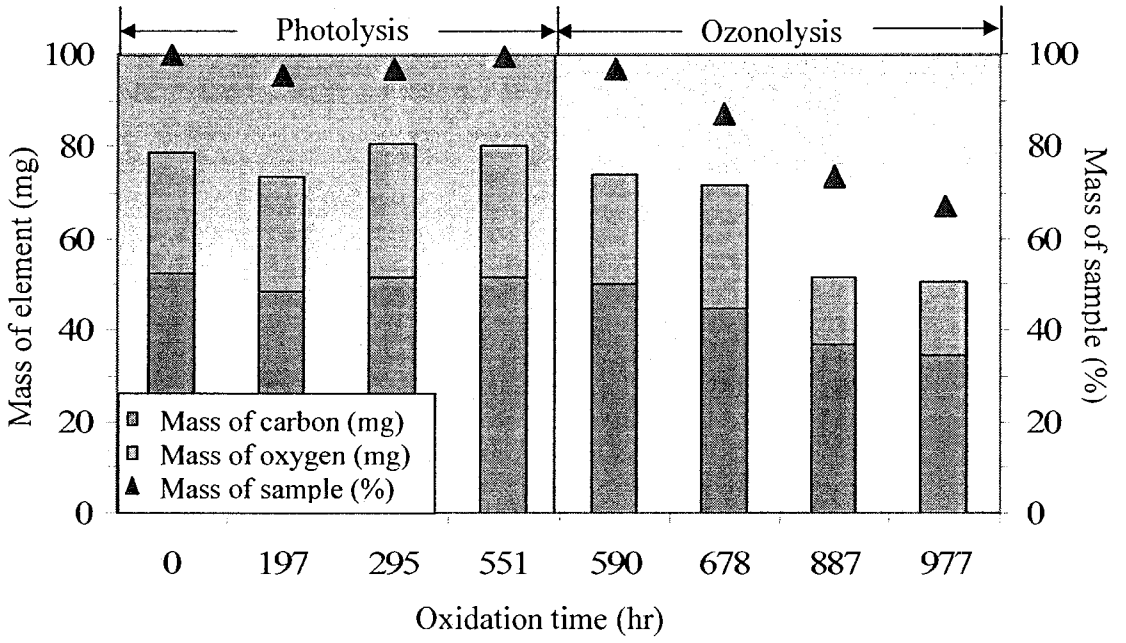

Figure 9. Changes in the total masses of carbon and oxygen during oxidation of melanoidin (initial mass of carbon = 52.7 mg, relative error = 0.692 % C, N = 5). The photolysis region represents exposure of the sample to UV radiation only, while the ozonolysis region represents exposure to elevated ozone levels.

Figure 9 presents the variation in the mass of carbon remaining at different time intervals during a melanoidin oxidation experiment. Small subsamples were taken from

the bulk sample at each time point and analyzed for its elemental composition. Only one aliquot of the sample was taken at each time point because of sample size restriction. The error, estimated at 0.4 mg C, was thus calculated from the analysis of five acetanilide standards inserted in the same run in parallel with the melanoidin samples. Surprisingly, the mass of carbon remaining after 197 hr of UV ray exposure is slightly lower than the mass remaining after 295 hr (48.5 ± 0.3 mg and 51.7 ± 0.4 mg C, respectively), which is technically impossible. The difference between the carbon mass at 197 hr and 295 hr is statistically significant, thus eliminating instrumental accuracy as the cause for the apparent increase in mass noted after 295 hr. The same phenomenon was also observed at that same time point for other BC samples run in parallel to melanoidin, which suggests that optimal combustion conditions may not have been reached during the elemental analysis of the samples exposed to UV radiation for 197 hr.

Complete combustion of graphite was also challenging since it is the most thermally stable BC component and the maximum combustion temperature available on the Perkin-Elmer elemental analyzer was of only 1050 °C. The highly polyaromatic structure making up the bulk of the graphene sheets in graphite explains this resistance to thermal oxidation since high temperatures and sufficient oxygen exposure time are needed to break the C=C bonds of the graphene sheet. Although the C=C bond order of graphite is equivalent to 1.3, its bond dissociation energy of 716 $kJ \cdot mol^{-1}$ corresponds to a bond order of 2.5. This high dissociation energy is partly due to the stabilization of the C-C bonds by resonance. Thus, even if most of the graphite is naturally formed at a lower temperature than the combustion temperature reached in the elemental analyzer, the

pressure under which it is formed compacts the structure to such a degree that oxidation of graphite requires some time to occur, even under such harsh oxidizing conditions as produced in an elemental analyzer. It is therefore not surprising to observe a small increase in C due to memory effects from one time point to the next, as seen in Figure 10 below.

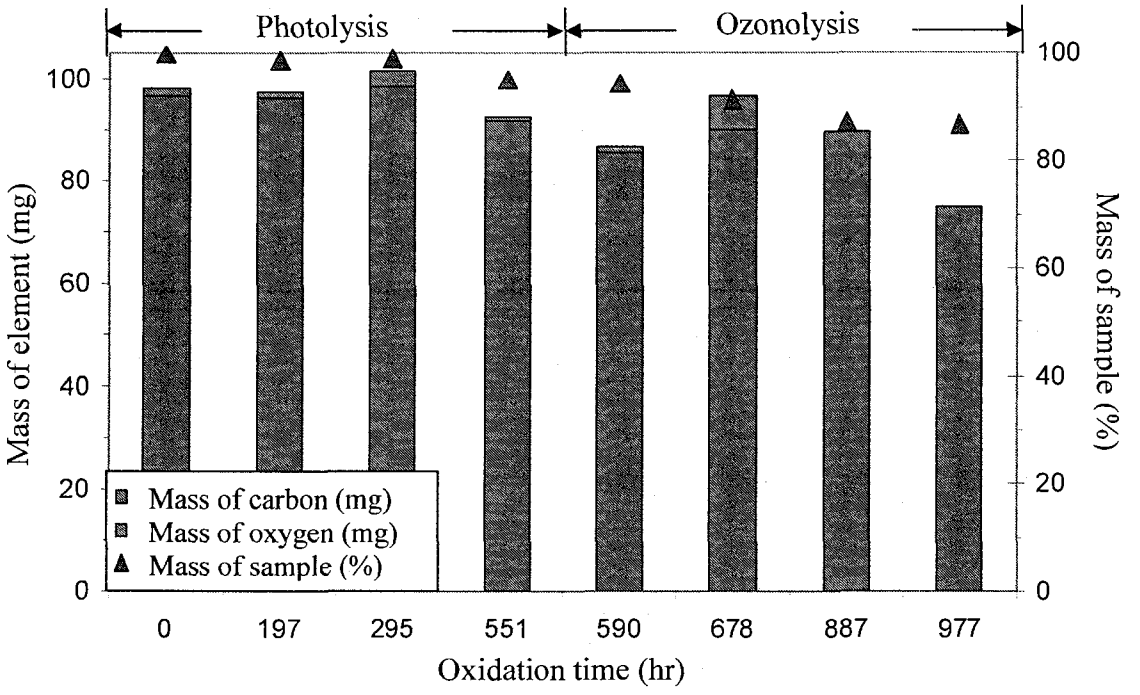

Figure 10. Changes in the total masses of carbon and oxygen during oxidation of graphite. (initial mass of carbon = 96.8 mg, see Figure 9 for an estimate of the relative error and population). The photolysis region represents exposure of the sample to UV radiation only, while the ozonolysis region represents exposure to elevated ozone levels.

Combustion of a sample into volatile gases can be compromised by strong polyaromatic bonds but also by the presence of minerals in a sample. Reduced minerals

like pyrite (FeS_2) are naturally present in marine sediments and are not removed by the chemical treatment performed on the sediments to isolate soot and graphitic carbon (Gélinas et al., 2001). These reduced minerals rapidly consume a large fraction of the molecular oxygen introduced into the combustion chamber during the combustion step and thus, less O_2 is available for the oxidation of the more slowly reacting BC compounds. Demineralization of the sediment with hydrofluoric acid also forms highly thermally stable solids like ralstonite ($NaAlMgF_6 \cdot H_2O$) and hieratite (K_2SiF_6), that can interfere with the combustion of BC components by consuming oxygen or entrapping organic components, thus decreasing O_2 accessibility.

A possible example of mineral interference can be seen in Figure 11, in which the variations in carbon mass of the Urban Particulate sample upon oxidation are presented. This sample comprises approximately 64 % of minerals on a mass basis, a fraction of which are assumed to contain elements in their reduced valence state (National Institute of Standards and Technology, Gaithersburg, USA).

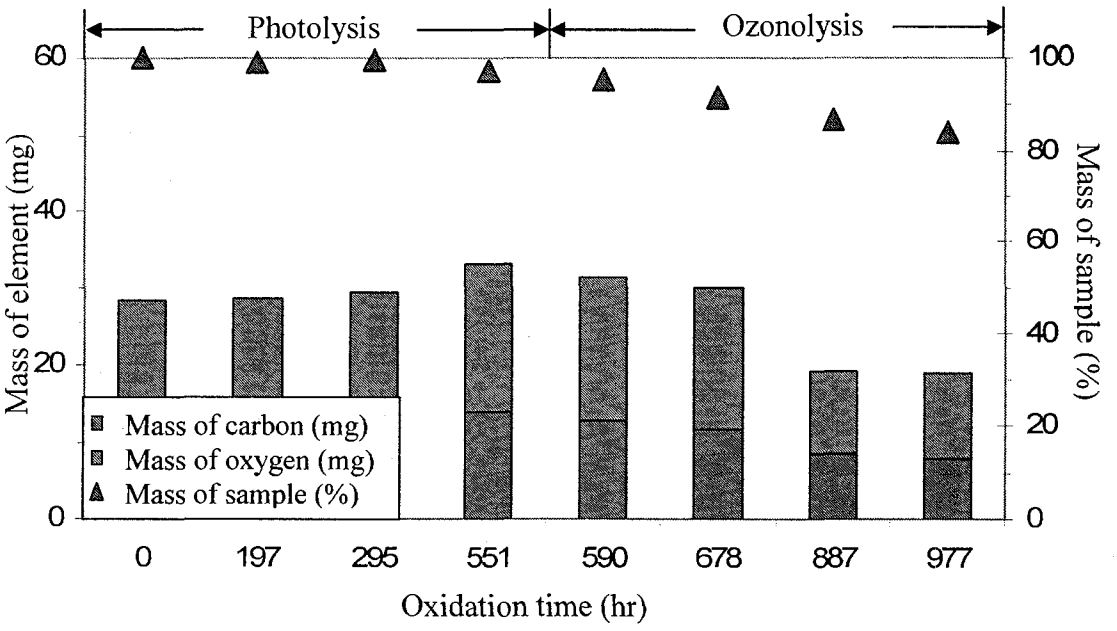

Figure 11. Changes in the total masses of carbon and oxygen during oxidation of Urban Particulate. (initial mass of carbon = 12.5 mg, see Figure 9 for an estimate of the relative error and population). The photolysis region represents exposure of the sample to UV radiation only, while the ozonolysis region represents exposure to elevated ozone levels.

As seen in this figure, there seems to be an increase in carbon mass between 0 and 295 hr of oxidation, followed by a constant decrease for longer oxidation times. The initial increase is impossible and can only be explained by an incomplete combustion of the sample or a memory effect occurring during the elemental analysis. Since Urban Particulate are composed in large parts of minerals (64 % w/w, National Institute of Standards and Technology, Gaithersburg, USA), a possible explanation to the increase in carbon mass is that an important fraction of the molecular oxygen introduced in the combustion chamber during the elemental analysis is consumed by reduced inorganic species/minerals, leading to an incomplete oxidation of the organic carbon. This is true for short exposure times to oxidizing conditions but as the oxidation time increases, the

proportion of the reduced inorganic species present in the sample that gets oxidized by the combustion decreases, thus increasing the amount of molecular oxygen available to combust the BC components.

While thermal oxidation of BC components in the presence of excess oxygen for the determination of carbon can sometimes prove difficult, the determination of the oxygen content in these samples is even more complicated. First, the precise and accurate pyrolytic measurement of BC is made difficult by the low natural abundance of oxygen in these components (the assumed main source of oxygen for the formation of CO_2 gas upon pyrolysis). Furthermore, the only parameter that can be optimized to increase the pyrolysis efficiency is temperature. However, even at the maximum operating temperature of 1050 °C, it remains very hard to completely oxidize these polyaromatic samples.

An example of imprecise pyrolysis could be observed from the results obtained for graphite, in Figure 10, in which there is an apparent increase in the mass of oxygen at 295 hr, and a sharp increase followed by a decrease at 678 hr. Since the quantities of oxygen measured in graphite are very close to the detection limit of the elemental analyzer (limit of detection and relative error of 0.09 mg O and 15.74 % for the time points of 0 hr to 678 hr, and 0.04 mg O and 8.83 % for the time points of 887 hr and 977 hr; limit of detections and relative errors differ between time points as the measurements for each time point were not performed during the same analysis), obtaining results with a poor precision is not surprising, especially with the added difficulty of the hard-to-pyrolyze

BC materials. In order to improve the precision of the results for oxygen-poor materials, Exeter Analytical Inc. suggested using hydrocarbon blanks to take into account the oxygen released from sources other than the sample during the analysis (Exeter Analytical, Inc, North Chelmsford, USA). The use of hydrocarbons as blanks could enable the quantification of CO_2 generated in the pyrolysis tube either through reaction with possible oxygen-containing contaminants in the platinized carbon or with the quartz tube itself.

Although it can be difficult to precisely quantify oxygen contained in BC components, the results obtained in this project show that oxygen measurements by elemental analysis can be used to qualitatively document the addition of oxygen on BC components as they undergo photolysis and ozonolysis. General reaction mechanisms of BC components with UV rays and ozone molecules can also be suggested based on changes of the oxygen content in BC components, as will be shown in Chapter 4.

2.4 Fourier-transform infrared analysis

Components of BC can sometimes prove difficult to analyse by FTIR spectroscopy because of the high absorptivity and albedo effect that characterize BC components. The absorptivity of BC material is much greater than in typical organic compounds because of their condensed polyaromatic structure that absorbs in much of the visible and IR, making the absorbance signal too strong to allow efficient detection of functional groups. It is therefore necessary to use a very small sample mass in order to increase transmittance of the incident beam and obtain FTIR spectra with interpretable peaks. An

example of a typical spectrum obtained from a sample containing 0.1 % of non-treated soot in KBr is shown in Figure 12.

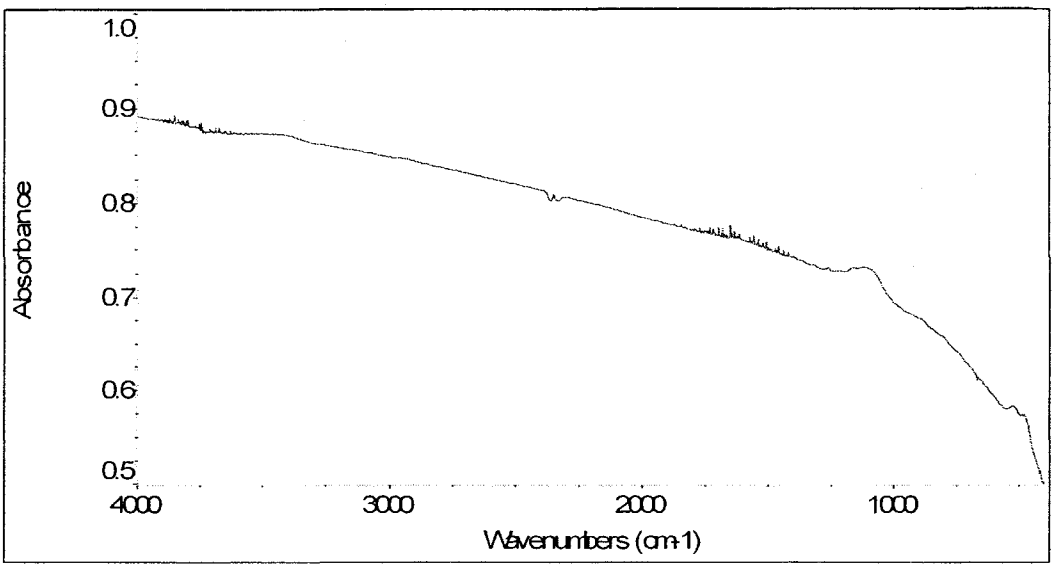

Figure 12. FTIR spectrum of a non-treated soot sample (0.1 wt% in KBr).

This figure clearly demonstrates the high absorptivity of soot with most of the absorbance signal (4000-1000 cm^{-1}) ranging between 0.7 and 0.9 AU despite the very high dilution factor of the sample with KBr. Absent from the spectrum are peaks from functional groups present in the molecular structure of soot, such as aromatics, carbonyls and hydroxyls (Akhter et al., 1985). This could be due to the combined effect of the high absorptivity of the sample and by the fact that FTIR spectroscopy only detects molecular functional groups present on the surface of highly condensed compounds such as soot and graphite. Alternatively, soot could also simply scatter, rather than absorb incoming electromagnetic radiations. Since most of the BC compounds are composed of polyaromatic clusters, IR rays are less likely to come into contact with small non-aromatic functional groups embedded within the structure, making the IR peaks even less

intense. It is to be noted that while the FTIR analyses for this project were performed with KBr pellets, most published FTIR data on BC compounds were obtained from thin films of *n*-hexane soot directly condensed on CaF_2 windows (Akhter et al., 1985; Smith & Chughtai, 1995) which allowed for a thinner and more uniform film than obtained with KBr pellets. Unfortunately, the FTIR scans of this project could not be performed following the same method since this procedure does not allow for oxidation kinetic studies on *n*-hexane soot as the sample cannot be removed from the window to perform other experiments.

Another technique that could have been used to detect changes in the chemical composition of BC components upon oxidation is attenuated total reflectance (ATR) spectroscopy. ATR is often used to scan the surface of samples or with samples of high absorptivity, like BC components. In ATR, the IR beam entering an optically dense crystal at the critical angle is reflected through the crystal, creating an evanescent wave. The attenuated energy from each wave penetrates the sample thus diminishing the intensity of IR rays reaching the sample and reducing the absorbance of the sample (Thermo Electron Corporation, Waltham, MA, USA)

During the course of this project, ATR trials with a crystal of ZnSe were done on some BC standards. However, the results obtained were not compiled because of a distortion in the IR spectra probably due to a refractive index of the crystal too close to that of the sample (refractive indices ZnSe: 2.4, graphite: 2.42 (Zhu et al., 2007)) or to the angle of incidence of the crystal being too low.

Complications arising when analyzing BC components by FTIR are also accentuated by the complexity of the macromolecular structure of the components, as explained in Chapter 1. The fact that BC components contain few functional groups (Akhter et al., 1985; Smith & Chughtai, 1995) attached to the polyaromatic ring clusters also contributes to the complexity of IR analysis because of the low abundance of the functional groups and the small fraction of these groups that are present on the surface of the material. A good example of the difficulties associated with FTIR analysis of BC compounds is given in Figure 13, which shows the area of an FTIR spectrum where peaks for aromatic functional groups are present (non-treated soot sample, 0.1 % in KBr). This spectrum suggests a very low abundance of aromatic groups in the compound, in contradiction with all previous publications on the polyaromatic molecular structure of soot (Akhter et al., 1985; Fernandes & Brooks, 2003; Fernandes et al., 2003; Kennedy, 1997; Smith & Chughtai, 1995; Stanmore et al., 2001). Despite the high aromaticity index of soot (0.9 to 1.0, (Akhter et al., 1985)), the scattering albedo effect seen with BC components, where a great amount of IR rays are reflected from the surface of the component back into the surrounding of the BC component, results in a poor representation of the chemical composition of the sample, identifying only a small fraction of aromatics (Smith & Chughtai, 1995).

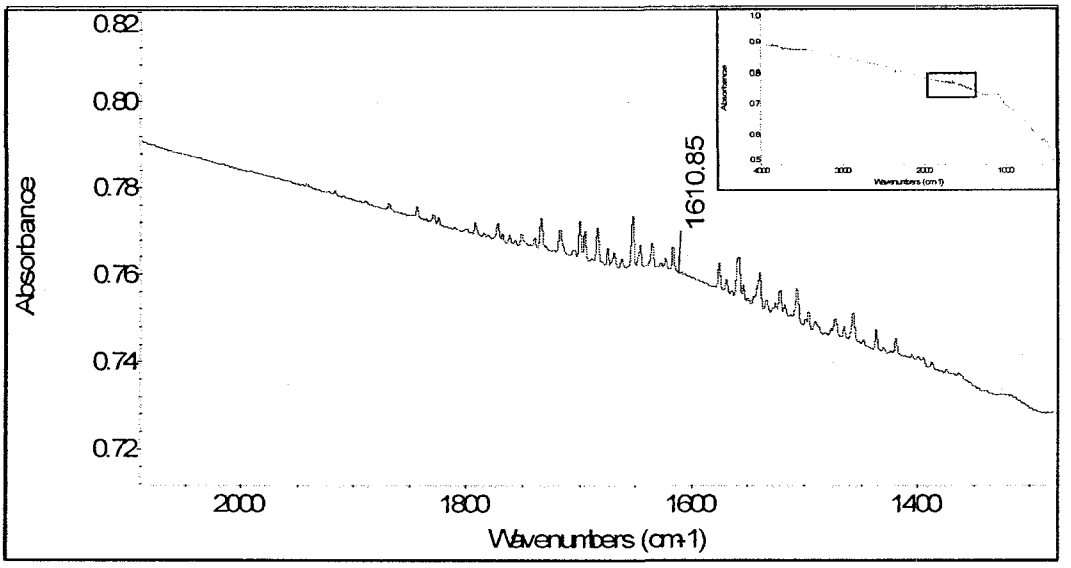

Figure 13. Expanded view of Figure 12 (non-treated soot, 0.1 % in KBr) showing the presence of aromatic groups

The poor representativity of FTIR spectra for these types of compounds is further demonstrated in Figure 14 below, which shows the range of frequencies where the most intense C-H stretching peaks are found (3000-2800 cm^{-1}; the spectrum is the same one as above: non-treated soot samples 0.1 % in KBr). Three small peaks attributable to aliphatics are evident at 2961, 2923 and 2853 cm^{-1}, with intensities that are close to those of the most abundant aromatic absorption peaks (aliphatics 2961 cm^{-1}: 0.0007 AU, 2923 cm^{-1}: 0.0008 AU, and 2853 cm^{-1}: 0.0005 AU; aromatic 1620 cm^{-1}: 0.0024 AU). Even though it is well known that the sensitivity for these aliphatic peaks is greater than that of the aromatic peaks, the much higher abundance of the aromatic functionalities in soot should have resulted in more intense absorption bands compared to those of the aliphatic moieties.

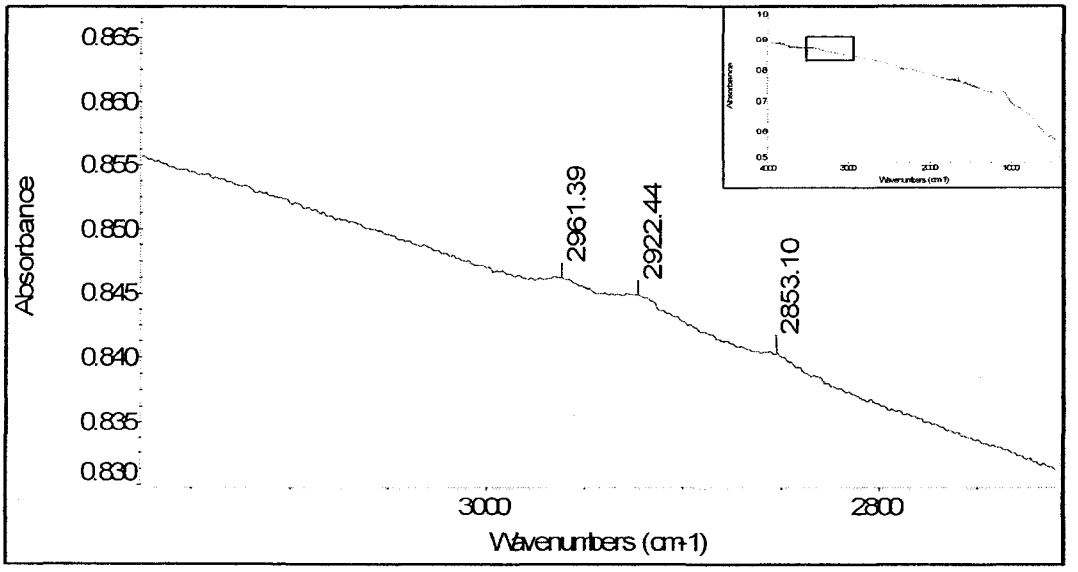

Figure 14. Expanded view of Figure 12 (0.1 % non-treated soot) showing the presence of aliphatic groups.

The high absorptivity of BC components resulted in diminished intensities for peaks from functional groups like aliphatics and carboxylic acids in such a way that it is impossible to use their peak heights to obtain quantitative or semi-quantitative information on the relative abundance of a given functional group. In order to decrease the background absorbance and heterogeneity of BC substances as well as to roughly quantify molecular changes in chemical composition between samples, Patrakov et al. used the calculated ratio of two different functional groups (Patrakov et al., 2006). Although this method does not allow for proper quantifications, it nonetheless provides information on the relative changes in functional group abundances. This approach could be useful for the characterization of chemical changes occurring upon oxidation, and thus, could provide valuable information on oxidation mechanisms. For example, the ratio of aliphatic groups over aromatics (sum of the absorbances at 2961, 2923 and 2853

cm^{-1}, over that at 1620 cm^{-1} is 0.83, 0.21 and 0.04 for non-treated, UV radiated and UV and ozone exposed soot, respectively). This decrease in aliphatic over aromatic groups indicates a change in molecular composition of soot throughout oxidation and suggests a preferential loss in saturated over aromatic groups most probably occurring because of the small relative abundance of aliphatics with respect to aromatics in BC materials.

Although FTIR spectroscopy cannot be used to quantify changes occurring in the chemical composition of BC components upon oxidation because of the high absorptivity and albedo effect of the samples, a qualitative measure of the changes can be obtained from the ratio of selected functional groups. The identification of molecular changes resulting from the oxidation helps in the determination of possible oxidation reactions.

3. Separation of soot and graphitic carbon by heavy-liquid density fractionation

Marine sediments contain a multitude of molecules with highly different functional groups. These include soot and graphitic carbon components deposited into the sediments by wind and river transport as well as through metamorphism, respectively (see Chapter 1). The possibility of specifically isolating each of these components from the bulk of the sedimentary organic "soup" would allow more detailed studies on the oxidation of each individual component under natural environmental conditions. While the isolation of soot and graphitic carbon from a natural sample can be achieved with a precision better than 15 % using a thermo-chemical method (Gélinas et al., 2001), there currently is no method that allows quantitative isolation of soot and graphitic carbon into separate fractions. Even though soot and graphitic carbon have two different formation pathways, they are structurally very similar and are thus inseparable from one another with common separation techniques such as preparative chromatography, liquid-liquid, or solid-phase extraction. Despite their similar structure and chemical composition, the sensitivity to (photo)chemical oxidation of soot and graphitic carbon differs considerably; while atmospheric soot is oxidized rapidly in the atmosphere (Druffel, 2004), graphite and graphitic carbon are considered highly resistant to oxidation (Gélinas et al., 2001). It is therefore very important to develop a method that allows separation of the two types of BC compounds, and to individually study their oxidation kinetics in order to evaluate their independent roles in the long-term reservoirs and fluxes of the Earth.

The insolubility of soot and graphitic carbon makes the development of a method to quantitatively separate the two BC compounds very difficult because most separation

techniques involve either the dissolution of one or both species in a liquid solution before separating them. However, one physical characteristic that differs considerably between these two BC compounds is their density, which can be exploited to physically separate them using heavy-liquid density fractionation (density of soot: 1.2 – 1.4 $g \cdot mL^{-1}$, Kim et al., 1999; 1.7 – 1.8 $g \cdot mL^{-1}$, Choi et al., 1995; density of graphite: 2.1 – 2.3 $g \cdot mL^{-1}$, Pierson, 1993). The heavy-liquid floatation procedure was previously used by Dickens et al. (2004) to estimate the ratios of combustion-derived BC (soot) and petrogenic graphitic carbon present in natural sediment isolates. The separation method, using sodium polytungstate as a heavy-liquid, was optimized and improved by down-scaling it to the micro-scale level to allow separation of very small quantities of the two BC compounds in a natural isolate (low microgram level).

A density of 1.8 $g \bullet mL^{-1}$ was chosen from the range of densities exhibited by the two BC compounds, as well as through visual evaluation of several separation trials (soot is composed of fine black particles while graphite is composed of coarser, metallic grey particles). However, since both soot and graphite (graphitic carbon) found in natural samples are not pure and comprise an array of macromolecules with varying degrees of alteration, traces of soot may be found mixed in with the graphitic carbon isolate (and *vice versa*). To ensure that optimal conditions were used for the separation of soot and graphitic carbon from natural sediments, the method was first validated with *n*-hexane soot and graphite standards. Since these two BC compounds have slightly different $^{13}C/^{12}C$ ratios, the evaluation of the separation efficiency was done using the stable carbon isotopic signatures of the original samples and that of the separated ones.

As explained in Section 2.3, the optimization of the combustion parameters of the elemental analyzer is critical in order to insure complete combustion of the samples being analyzed. However, one of the essential parameters for optimal combustion conditions, the combustion time, cannot be adjusted on the Eurovector EA as it was on the Perkin-Elmer EA. Thus, even though the oxygen input rate (and thus the amount) was increased to match the optimized parameters of the Perkin-Elmer instrument, the time that the sample is bathed in a hot and oxic atmosphere would have to be increased on the Eurovector EA to compensate for the slow thermal oxidation kinetics of graphite. However, despite the possibly incomplete combustion of graphite on the EA coupled to the IRMS, the isotopic signature of graphite samples should not be altered significantly since the distribution of the ^{13}C isotopes in the crystalline structure of graphite is uniform.

Table 2 shows six different mixtures of *n*-hexane soot and graphite standards separated with sodium polytungstate. The separation trials were performed using a range of initial masses of standards in a ratio of approximately 1:1. This trial was carried out to estimate the efficiency of the separation method and the minimum sample mass that can be efficiently separated using the optimized micro-scale method. The separation efficiency can be assessed by measuring (*i*) the total mass of each separated fraction (mass balance approach), (*ii*) the carbon mass in each separated fraction (carbon mass balance approach), or (*iii*) the stable isotope ratios of the standards, the mixture and the separated fractions (isotopic mass balance approach). The first two approaches have the disadvantage of not being specific to either one of the BC compounds. In the first case, even the sum of the BC compounds remains uncertain (i.e., residual salts can affect the

mass balance calculations), whereas the third one, while being specific to each BC compounds, most likely is less precise since the difference between the stable carbon isotope ratio signatures is small (pure *n*-hexane soot: -24.01 ± 0.30 ‰, pure graphite: -22.69 ± 0.14 ‰). All three parameters were used to assess the efficiency of the separation in these trial runs.

Table 2. Method validation for the heavy-liquid separation of soot and graphite

Trial sample	Mass recovery (%)	$\delta^{13}C$ (‰)	OC† based on		Standard Deviation	
			C mass (%)	$\delta^{13}C$ (%)	%OC (‰)	$\delta^{13}C$ (‰)
1 Mixture		-23.03				
Soot	98	-23.69	56 (51)‡	34	9.2	11
Graphite	46	-22.66	44 (49)	66		
2 Mixture		-23.27				
Soot	105	-23.71	51 (51)	54	2.0	39
Graphite	97	-22.67	49 (49)	46		
3 Mixture		-23.19				
Soot	99.4	-23.65	52 (50)	30	0.3	13
Graphite	124	-22.88	48 (50)	70		
4 Mixture		-23.17				
Soot	30.0	-23.56	58 (51)	29	8.3	14
Graphite	513	-23.03	43 (49)	71		
5 Mixture		-22.66				
Soot	133	-22.40	56 (51)	29	1.8	107
Graphite	135	-27.63	44 (49)	71		
6 Mixture		-22.66				
Soot	139	-22.38	48 (50)	67	2.3	9.6
Graphite	231	-22.87	52 (50)	33		

†With respect to total organic carbon ‡Percent separated phases expected

A large volume of water is needed to rinse the recovered standards and wash away the remaining sodium polytungstate salt. For a fractionation that was about 4 mL of heavy-liquid, a volume of about 200 mL of rinsing water was used to remove the salt. However, the calculated mass balances still indicates the presence of remaining salts for some of the collected standards with recoveries as high as 513 %. While this salt would probably not interfere with carbon-based or isotope-based measurements, it shows that simple mass balance calculations cannot be used to estimate the recovery of each standard.

Another element revealed by the mass recoveries during the trial runs is a loss of sample during the fractionation procedure with, for example, a recovery as low as 30.0 % for *n*-hexane soot in Trial 4. This low recovery indicates a loss of soot either because of an inefficient fractionation (in which case the lost soot would be collected with the recovered graphite and hence increase the mass recovery of the latter), or to the adsorption of soot onto the wall of the eppendorf tube used to fractionate the mixture. During the course of the method development, polyethylene eppendorf tubes were substituted for tubes coated with silicon to reduce the adsorption of soot and graphite onto the wall of the tube.

Standard deviations of isotopic signatures for the separated mixtures were calculated based on either two or three aliquots (when possible) and fall between the range 0.003 – 0.68 ‰. While such low standard deviations indicate a precise measurement of the isotopic ratios, the fact that the measured $\delta^{13}C$ signatures for the soot

and graphite fractions isolated by heavy-liquid floatation are very close (difference of only 0.53 ‰ in Trial 4 for example) strongly limits the discrimination power of the stable isotope approach. Because of the similarity in initial isotopic signature between the two standards, very small differences in isotopic ratios measured for the separated fractions lead to large differences in the calculated percentages of each standard in the mixture. For example, in Trial 5, the standard deviations of the isotopic signatures of the mixture and soot (mixture: n = 3; soot: n = 3; graphite: n = 1) are 0.67 and 0.38 ‰, respectively. This leads to a difference in the calculated percentages of each fraction corresponding to a standard deviation of 107 %. A much better precision in stable carbon isotope measurements by EA-IRMS would be needed to be able to use the isotopic signature approach to satisfactorily quantify soot and graphitic carbon isolated from natural samples by heavy-liquid floatation. Alternatively, standards with larger differences in isotopic signatures, such as meteorite graphite or soot from C4 plants could have been used to validate the method ($\delta^{13}C \sim$ -8 ‰, and from -10 ‰ to -16 ‰ for meteorite graphite and C4 plants respectively, (Clark & Fritz, 1997)).

While the best way to calculate the percent recovery of soot and graphite seems to be with the carbon mass balance, the stable carbon isotope signature of the recovered fractions is a valuable tool as it discriminates between soot and graphite. The specificity of the isotopic signature can be observed when comparing Trials 2 and 5. The percent carbon of each fractionation indicates a good separation with 51 % and 56 % soot and 49 % and 44 % graphite, respectively. However, the carbon isotopic signature of the two fractionations indicates that Trial 2 was more efficient since the calculated organic carbon

based on the isotopic ratios is better for Trial 2 (with standard deviations of 39 and 107 ‰ for Trials 2 and 5, respectively). This result therefore indicates an exchange of soot and graphite in the phases of Trial 5 that the percent carbon could not detect. A combination of the two methods, carbon mass balance and isotopic mass balance therefore remains the best approach.

Isolated soot and graphitic carbon from natural sediments were also fractionated using sodium polytungstate. The results obtained for a series of five samples are presented in Table 3 and compared with data from published studies on the graphitic carbon isolates from the same sediments using different techniques of analysis.

Table 3. Heavy-liquid fractionation of soot and graphitic carbon from natural sediments

Sediment	†Sample	Initial mass (mg)	$\delta^{13}C$ (‰)	Relative contribution (% of OC in isolate)
Stillaguamish River	Mixture	30.4	-24.08	
	Soot		-25.66	7.6
	G. carbon		-23.95	92.4
Saguenay River Station 30	Mixture	69.7	-25.71	
	Soot		-25.69	81.6
	G. carbon		-25.73	18.4
SRM 2740 Buffalo River	Mixture	68.3	-24.11	
	Soot		-23.99	69.6
	G. carbon		-24.38	30.4
Lake Washington	Mixture	15.7	-23.56	
	Soot		-24.09	40.8
	G. carbon		-23.19	59.2
Arctic Shelf	Mixture	30.1	-25.98	
	Soot		-24.45	13.0
	G. carbon		-26.21	87.0

†G. carbon stands for graphitic carbon

Comparison of the results shown in Table 3 with published data demonstrates the high potential of this improved method of fractionation to quantify soot and graphitic carbon in natural samples. Stillaguamish River, the sediment used in this study, drains

the Cascades Mountains north of Seattle (WA, USA). The sampling site is located in a remote area, far from any urbanized center and downwind from the Pacific Ocean (Dickens et al., 2004). Very little soot was thus expected to be found at this site. The results obtained by heavy-liquid floatation indicate that 92.4 % of the carbon from the graphitic BC isolate is locked up in graphitic carbon structures. This result also agrees with a recent study on the same sediment sample performed by Haberstroh et al. (2006) using carbon X-ray absorption near-edge structure spectroscopy and scanning transmission X-ray microscopy and in which the contribution of highly ordered and impure graphitic carbon was found to be over 80 %.

A strong predominance of graphitic carbon over soot was also expected for the isolated residue of the Arctic Shelf sediment collected in the vicinity of the MacKenzie River delta since the area is far from any urbanized/industrialized center. Goñi et al. (2005) also reported that about 70 % of the carbon found in these sediments was composed of fossil organic carbon originating from soils and rock formations, which constitute the sources for graphitic carbon. The greater contribution of graphitic carbon in the isolate of the Arctic Shelf sediment measured in our study (87.0 % and 13.0 % for graphitic carbon and soot, respectively) is in agreement with the findings of Goñi et al.

The other three samples were expected to be enriched in soot compared to graphitic carbon. The sediment from the Saguenay Fjord (Quebec, Canada) was sampled in an area affected by frequent forest fires and by aluminium smelters, both of which are known to emit large quantities of soot, while the sample from the Buffalo River was

collected in the industrialized downtown area of Buffalo (NY, USA). Lake Washington is located in Seattle (WA, USA), downwind from the city downtown and industrial areas. Dickens et al. used a large-scale sodium polytungstate heavy-liquid fractionation scheme on whole sediments and estimated that soot accounted for 73 % of the graphitic BC isolate at this site (Dickens et al., 2004). The results obtained in our study (81.6, 69.6 and 40.8 % for the Saguenay Fjord, Buffalo River, and Lake Washington, respectively) are in agreement with the expected or measured composition. The slightly higher soot contribution found by Dickens et al. is most likely due to the fact that a cut-off density of 2.0 $g \cdot mL^{-1}$ was used in that study compared to our cut-off of 1.8 $g \cdot mL^{-1}$.

Heavy-liquid sodium polytungstate was proven to be an efficient tool to separate soot and graphitic carbon from natural sediment samples. The technique enables the fractionation of soot and graphitic carbon present in natural sediment samples without affecting the chemical structure of the two phases, thus allowing the possibility for further study of the separate phases of soot and graphitic carbon.

Although conventional analytical techniques cannot be exploited to analyze the macromolecular and highly refractory BC components studied in this project, other approaches such as elemental analysis, FTIR and thermogravimetry can provide invaluable clues on changes in the chemical composition of BC components upon oxidation. The complementarity of the techniques result in a broad range of analytical information that can be used to at least qualitatively evaluate structural changes occurring in a given BC sample during photo- and chemical oxidation. Analytical difficulties

associated with these atypical samples remain however present, and thus great precaution should always be taken to obtain good analytical results.

4. Oxidizability of soot and graphitic carbon

The BC continuum is composed of many BC compounds covering a wide range of aromaticity and reactivity. Soot and graphitic carbon, produced through the gas phase condensation of volatile residues emitted during the combustion of biomass or fossil fuels and from metamorphism, respectively, are generally assumed to be among the most refractory BC components. However, soot has been shown to be UV-sensitive in the atmosphere, producing a series of carboxylic and dicarboxylic acids upon oxidation (Smith & Chughtai, 1995). Furthermore, pure graphite can also be oxidized under certain conditions (Apatiga et al., 2002; Backreedy et al., 2001; Langley et al., 2006) and it is not clear yet whether graphitic carbon is totally inert or if it is oxidized to some extent when exposed to UV and/or ozone over very long time scales in natural environments. An assessment of their reactivity to UV radiation and ozone could improve the understanding of the role of soot and graphitic carbon in the global carbon cycle and in particular in the sink component of the global carbon mass balance equation. However, the measurement of the oxidizability of soot and graphitic carbon can prove difficult due to their macromolecular structure and chemical refractoriness, which prevent the use of conventional spectroscopic or chromatographic methods that require dissolution of the analyte. The oxidizability of these refractory BC compounds must thus be assessed using indirect investigation methods.

Molecular transformations occurring during oxidation of BC compounds by UV radiation and ozone exposure result in a mass change that can be monitored through elemental mass balance calculations and thermogravimetry. For example, Leifeld

recently demonstrated that pure BC standards such as graphite and *n*-hexane soot can be distinguished using differential thermogravimetry (Leifeld, 2007) . In this chapter, the use of these indirect methods for the assessment of the oxidizability of a series of pure BC standards and BC isolates from natural sediments are reported. The potential determination power of DTA to quantify the abundance of soot and graphitic carbon present in natural graphitic carbon isolates is also investigated. In addition, mechanisms of oxidation of soot and graphitic carbon are proposed based on analytical results.

4.1 Oxidation of BC and natural samples

Oxidation of BC compounds by ozone was previously reported to form hydrophilic functional groups such as carboxyl and phenol (Swann & Evans, 1979), as well as carbonate, lactone, peroxide and anhydride (Mawhinney & Yates, 2001). These newly formed functional groups increase the hydrophilicity of BC compounds and lead to the release of small volatile organic molecules, thus contributing to their abiotic degradation. This degradation pathway can be monitored through the measurement of the elemental composition of BC compounds at different time points during their oxidation, as well as through thermogravimetric analyses of the compounds before and after oxidation, which can provide information on the loss of organic carbon and the formation of oxygen-containing functional groups.

The elemental composition of the different BC samples was thus monitored throughout the oxidation experiment to evaluate their relative oxidizabilities (Figure 15). In general, the loss of carbon, as a percent of the initial mass, agrees with the expected

relative labilities of the BC components, with a greater loss of carbon for the more labile components (oak, urban particulate, melanoidin and the Stillaguamish River isolate, with remaining carbon percentages of 51.0, 63.8, 65.9 and 20.8 % after 977 hrs of oxidation, respectively). While the greater labilities of oak, urban particulate and melanoidin can be explained by their low degrees of crystallinity (Braun et al., 2001; Nunes & Coimbra, 2007), that of the Stillaguamish River isolate is probably due to the low initial mass of the sample. Indeed, the sample mass of the isolate goes from 2.7 mg to 0.6 mg organic carbon compared to 46.7 mg to 23.8 mg, 12.5 mg to 8 mg, and 52.7 mg and 34.7 mg for oak, urban particulate and melanoidin after 977 hrs of oxidation, respectively (see Table 4 for more details). Sample availability limited the mass of the Stillaguamish River isolate that could be used in any single experiment.

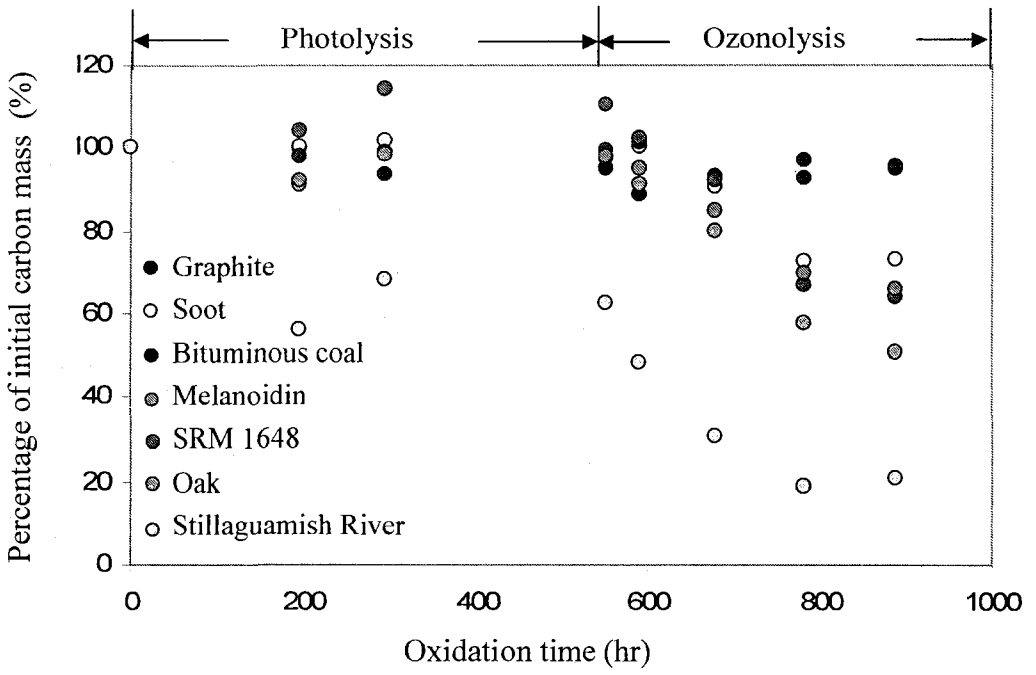

Figure 15. Changes in carbon mass remaining during oxidation for different BC samples. (initial masses of samples: about 100 mg, initial carbon masses: graphite = 96.8 mg; *n*-hexane soot = 90.7 mg; bituminous coal = 70.0 mg; melanoidin = 52.7 mg; Urban particulate = 12.5 mg; oak = 46.7 mg; Stillaguamish River isolate = 2.7 mg, see Figure 9 for an estimate of the relative error and population). The photolysis region represents exposure of the sample to UV radiation, while the ozonolysis region represents exposure to ozone.

Table 4. Changes in total masses of carbon and oxygen (mg) in BC samples during oxidation

Sample	Element (mg)	Oxidation time			% Change
		0 hr	551 hr	977 hr	
Graphite	Carbon	96.8 (100)†	91.8 (94.8)	91.7 (94.7)	-5.27
	Oxygen	1.4 (100)	0.9 (64)	0.0 (0)	-100.0
n-Hexane Soot	Carbon	90.7 (100)	88.5 (97.6)	66.1 (72.9)	-27.1
	Oxygen	5.5 (100)	2.0 (36)	12.0 (218)	+118
Bitiminous Coal	Carbon	70.0 (100)	69.3 (99.0)	66.8 (95.4)	-4.57
	Oxygen	8.8 (100)	8.0 (90)	6.5 (74)	-26
Urban particulate (SRM 1648)	Carbon	12.5 (100)	13.8 (110)	8.0 (64)	-36
	Oxygen	15.6 (100)	19.2 (123)	10.8 (69.2)	-30.8
Melanoidin	Carbon	52.7 (100)	51.6 (97.9)	34.7 (65.8)	-34.2
	Oxygen	26.0 (100)	28.4 (109)	16.0 (61.5)	-38.5
Oak	Carbon	46.7 (100)	45.3 (97.0)	23.8 (51.0)	-49.0
	Oxygen	38.5 (100)	41.4 (108)	19.3 (50.1)	-49.9
Stillaguamish River	Carbon	2.7 (100)	1.7 (63)	0.6 (22)	-78

†Numbers in parentheses are percent element (carbon or oxygen) remaining

The mass of carbon remaining for *n*-hexane soot (72.9 % of initial C) indicates high reactivity towards ozonolysis for this component despite its high average molecular weight and macromolecular structure, suggesting the presence of hydrophilic sites where

ozone molecules can attack the soot structure, as reported elsewhere (Akhter et al., 1985; Kennedy, 1997; Zuberi et al., 2005). As discussed in more details in Section 2.3, the increase in carbon mass observed in Urban Particulate Matter is probably due to the incomplete oxidation of the sample at time 0 hr because of the consumption of oxygen by reduced inorganic species originally present in the sample. On the other hand, while the oxidizability of soot by ozone was expected, the results obtained for graphite and bituminous coal were surprising: Graphite, which is generally assumed to be highly refractory and almost impossible to degrade under normal environmental conditions, was oxidized to 94.7 % of its original carbon content. In contrast, bituminous coal, expected to decompose at a rate similar to that of *n*-hexane soot owing to its relatively low initial carbon percentage (70.0 %) and the presence of oxygen-containing groups in its structure, was only oxidized to 96.8 % of its original carbon concentration (see Figure 16 for more details on the oxidation of bituminous coal). Although the structure of a component can often be linked to its resistance to oxidation, in the particular case of coal the influence of the chemical composition and physical structure on its susceptibility to photochemical oxidation remains a source of debate (Wang et al., 2003). Furthermore, as reported recently, the rate of consumption of oxygen for a weathered or oxidized coal is much lower than for a fresh coal sample (Krishnaswamy et al., 1996; Wang et al., 2003). Therefore, it is possible that the bituminous coal sample used in this project was partly oxidized upon collection, or that it had begun oxidizing under normal room conditions in such a way as to decrease the oxidation rate during the experiment (the sample was acquired more than 10 years ago). It has been suggested that the accumulation of oxygenated functional groups formed during oxidation of bituminous coal on the internal

surface of pores hinders oxygen access to the interior of the coal particles, thus partially inhibiting further oxidation (Wang et al., 2003). Hence, it is plausible that specific characteristics of the bituminous coal sample such as pore and particle size, or gases entrapped within the particles may have affected its oxidation kinetics.

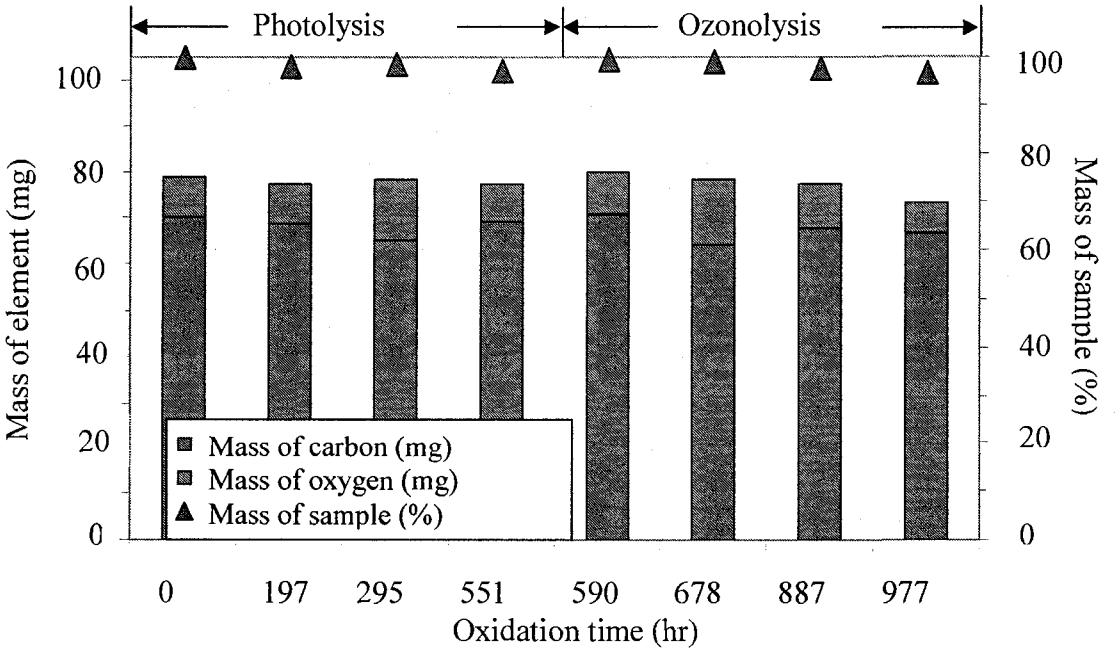

Figure 16. Changes in elemental composition and sample mass during oxidation for bituminous coal (initial carbon mass = 70.0 mg, see Figure 9 for an estimate of the relative error and population). The photolysis region represents exposure of the sample to UV radiation, while the ozonolysis region represents exposure to elevated ozone levels.

The limited impact of photolysis and ozonolysis on the molecular structure of bituminous coal can also be observed in the DTA thermograms of the sample obtained before and after its oxidation. The formation of more labile compounds from refractory

parent material is usually accompanied by a shift in the low temperature boundary of the main peak to a lower temperature, corresponding to molecular structures that are more thermally labile. Two thermograms of bituminous coal obtained before and after oxidation by UV ray and elevated ozone exposure are shown in Figure 17. The DTA analyses corroborate the results obtained through elemental analysis by showing that the oxidation lead to very small molecular changes, thus supporting the very small loss of carbon observed. This can be seen by the almost identical DTA thermograms of the component obtained before and after its oxidation.

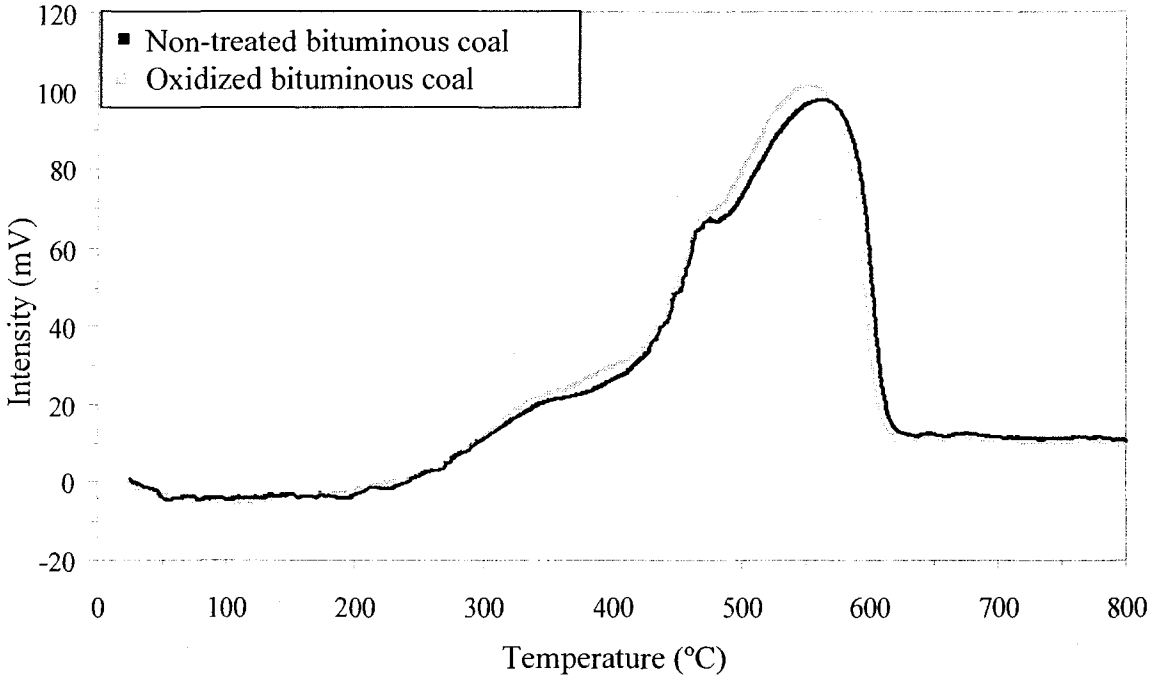

Figure 17. Changes in thermal resistance of bituminous coal following oxidation

The highly refractory nature of graphite and its resistance to oxidation under normal environmental conditions are thought to be linked to the absence of electrophilic groups

in its molecular structure as they reduce the molecular strain of a molecule (Kwiecinska & Petersen, 2004). However, the oxidizability of the graphite sample studied in this project was surprisingly greater than anticipated with an observed relative carbon loss of 5.27 %, as seen in Table 4.

While oxidation by UV radiation and ozone resulted in a significant loss of carbon (5.27 % loss of C), a comparison of the thermograms of graphite obtained before and after oxidation suggests only a slight change in molecular structure. These newly formed molecules or functional groups on the graphite backbone can be observed in the temperature range of 160 °C to 440 °C, as seen in Figure 18. The small change in molecular structure accompanied with a carbon loss of 5.27 % suggests that the oxidation of graphite occurs mainly through the production of volatile gases such as carbon monoxide and carbon dioxide (Backreedy et al., 2001; Hahn, 2005; Lerf et al., 1998).

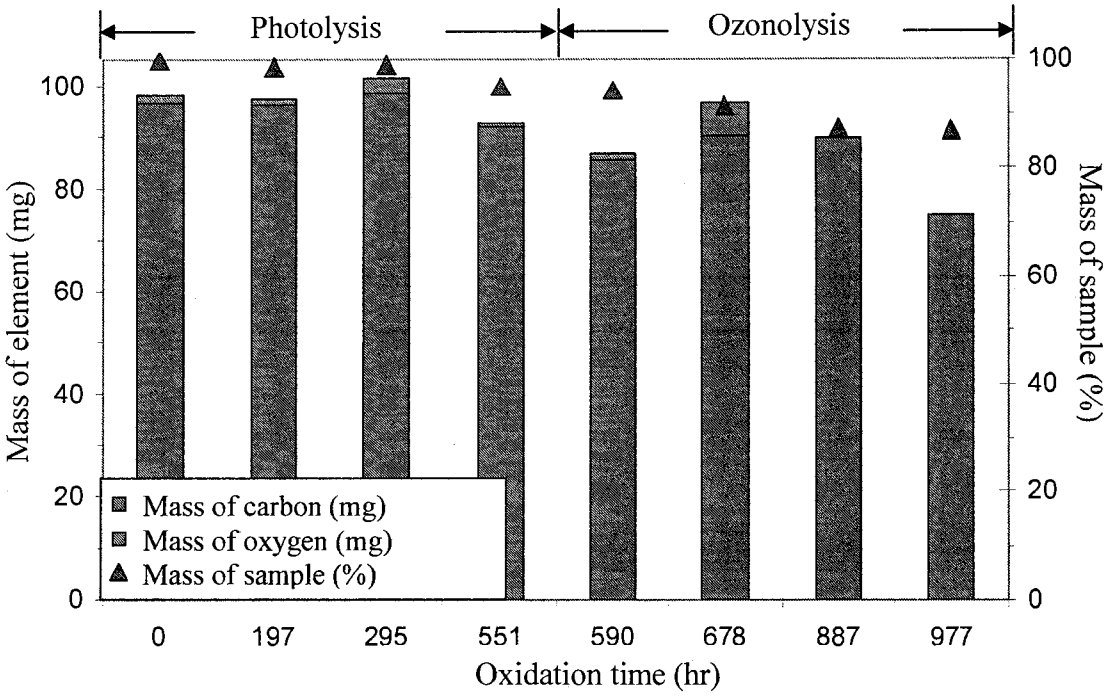

Figure 18. Changes in the total masses of carbon and oxygen during oxidation of graphite (initial carbon mass = 96.8 mg, see Figure 9 for an estimate of the relative error and population). The photolysis region represents exposure of the sample to UV radiation, while the ozonolysis region represents exposure to elevated levels of ozone.

A possible explanation for the observed ozonolysis of graphite is the presence of a delocalized pi electron system that could enable ozone to react with some of the double bonds through an electrophilic reaction. Such a reaction was proposed by Li et al. (2006) in which a fault line is created by the formation of oxirane bonds aligned in a straight line on a graphene sheet where further oxidation can take place. The proposed mechanism is shown in Figure 19 below.

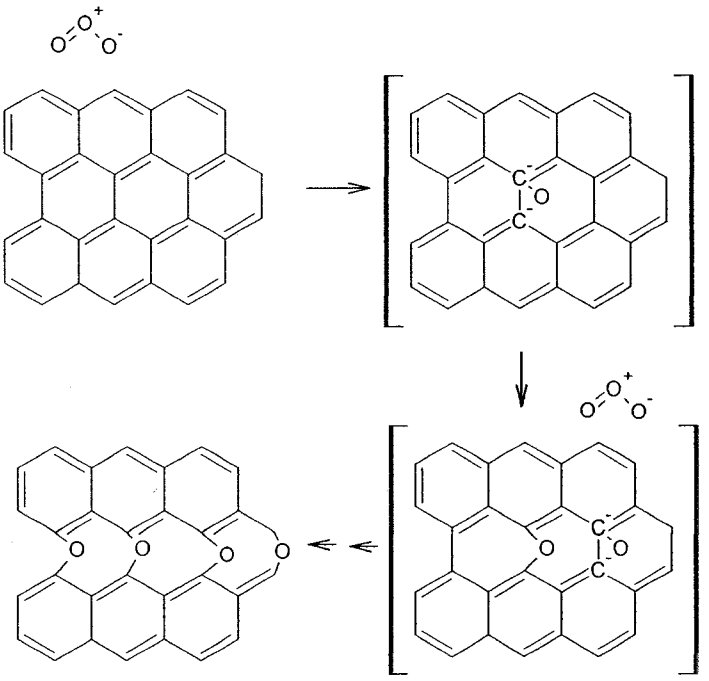

Figure 19. Proposed mechanism for the oxidation of graphite (Li et al., 2006)

This proposed mechanism shows the formation of oxirane bridges along the backbone of the graphene sheet, distorting the planarity of the graphene layer due to a transformation of the C hybridization from sp^2 to sp^3. The distortion also causes a weakening of the C bond adjacent to the oxygen, thus increasing the possibility of further reactions with oxygen. Although not represented in this mechanism, the formation of oxirane groups occurs when the active carbon sites at the edges of graphenes are oxidized since atomic oxygen reacts preferentially with these carbon sites (Sanchez & Mondragon, 2007). This suggests that the oxidation of the graphite sample began primarily with the oxidation of the carbon active sites located at the edge of the structure, thus minimizing the major structural changes that would lead to thermogravimetric alterations of the oxidized sample. Although the thermogravimetric similarities between the original and the oxidized samples of graphite, as seen in Figure 20, suggests only a small change in

molecular structure during oxidation, a small amount of newly formed molecules can, however, be observed between 160 °C and 440 °C in the thermogram of the oxidized graphite. These thermally more labile molecules most likely are not enriched in oxygenated functional groups since the contribution of oxygen to the total mass of graphite remained relatively stable throughout oxidation (see Table 4 above). It is therefore probable that the newly formed molecules were produced from the opening of larger graphene sheets through the formation of oxirane groups.

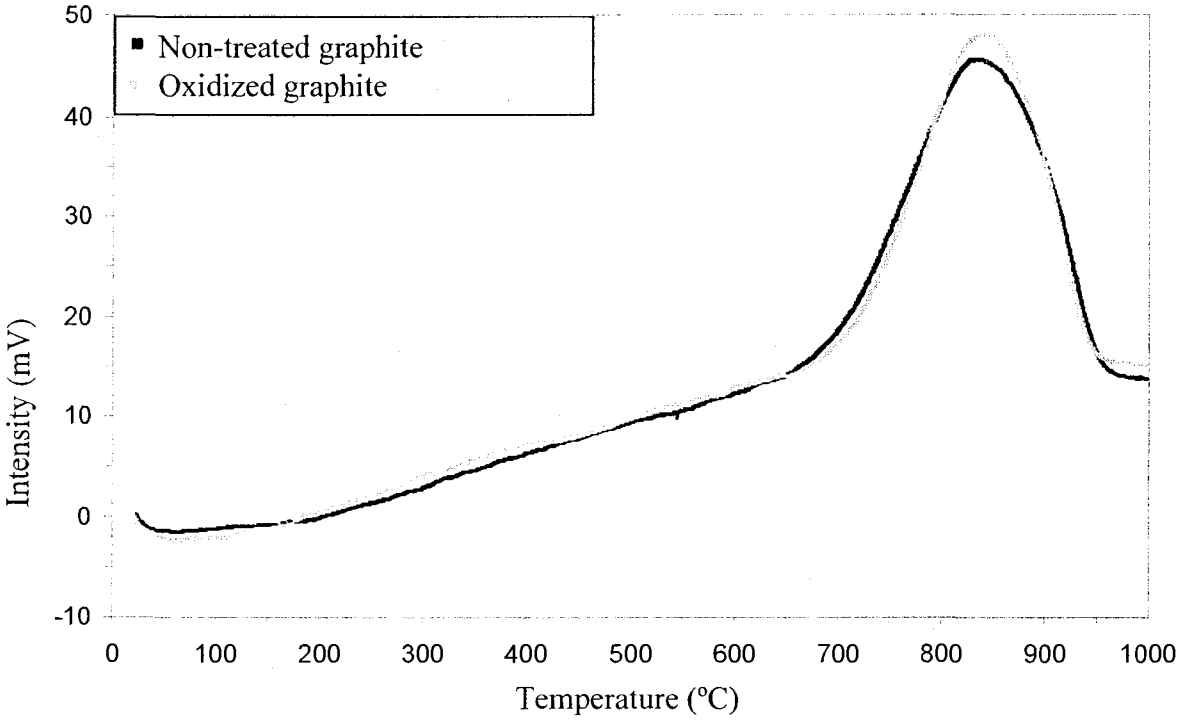

Figure 20. Changes in thermal resistance of graphite following oxidation

The oxidation of graphite unexpectedly resulted in a small oxygen mass loss from 1.4 mg O to undetectable levels. This small oxygen loss, combined to a carbon mass loss of 5.27 % (from 96.8 to 91.7 mg C) and a small molecular structure change further

support the hypothesis of an oxidation of graphite that starts from the edges of the structure since an opening of the graphene sheets through the formation of oxirane bonds would produce smaller graphene units with a higher density of carbon active sites ready to react with oxygen and hence increase the formation of more labile molecules. The smaller graphite units would also produce thermogravimetric changes observable in DTA. On the other hand, other graphite oxidation mechanisms minimizing the production of small labile molecules by the formation of CO and CO_2 as primary products of graphite oxidation have been proposed (Backreedy et al., 2001; Hahn, 2005; Lerf et al., 1998). For example, Backreedy et al. (2001) proposed an oxidation pathway for graphite in which the bulk of the molecular structure remains relatively unchanged until it is attacked, through the oxidation of the surface layers, by ozone and oxygen molecules. The attack on the graphite structure would thus come from the outside of the molecule (Backreedy et al., 2001). This mechanism, shown in Figure 21, is in good agreement with the thermogravimetric results obtained in this project as an attack of molecular oxygen and ozone molecules starting from the outside of the graphite sheet would result in little changes in the bulk of the graphite sheet structure. Although this mechanism seems to corroborate results obtained through differential thermogravimetry, it is highly probable that the mechanism presented above (Figure 19) also plays a role in the oxidation of graphite, along with the mechanism of Figure 21 and several others that have yet to be fully characterized.

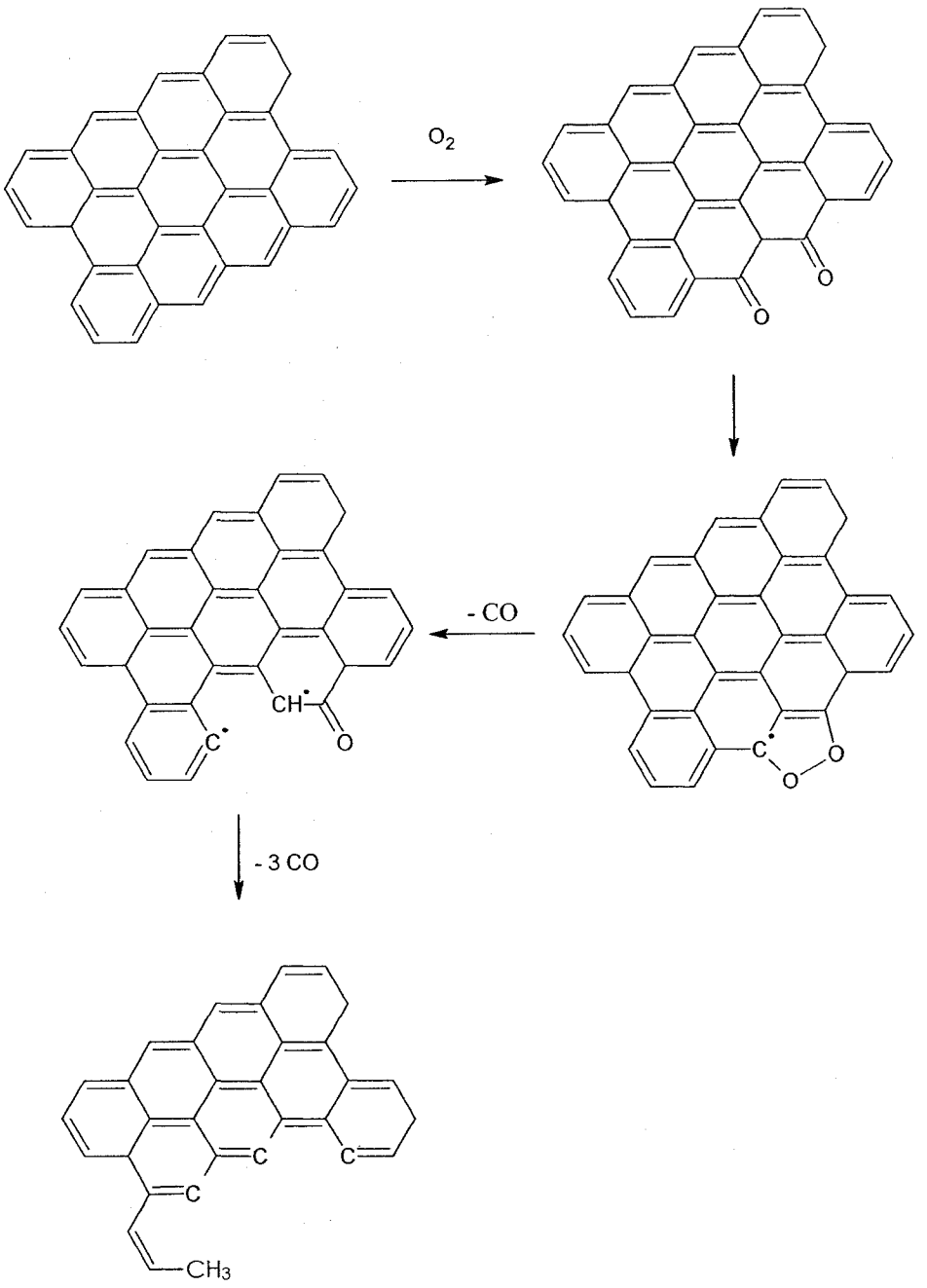

Figure 21. Alternative mechanism for the oxidation of graphite as proposed by (Backreedy et al., 2001)

This graphite oxidation pathway primarily produces carbon monoxide and carbon dioxide gases because of the compact structure of graphite and its lack of oxygenated

functional groups within the graphene sheets. Since the other BC components are produced from combustion of biomass and fossil fuel, their structures, although also of macromolecular sizes, are less compact and contain a higher abundance of oxygen-containing functional groups that are present both inside and on the edges of the structure, thus enhancing their oxidation rate. The role of ozone in the oxidation of BC materials is particularly noticeable for *n*-hexane soot for which the loss of carbon during ozonolysis was greater than for photolysis by about an order of magnitude (10.2 times greater). The importance of ozone was further demonstrated by the decrease in O/C molar ratio from 0.05 to 0.02 during photolysis (from 0 to 551 hrs), to reach a ratio of 0.14 after ozonolysis (after 977 hrs) of the *n*-hexane sample, thus indicating a significant intake in oxygen during the last oxidation phase.

The function of ozone in the degradation of *n*-hexane soot has been widely investigated. It is generally accepted that oxygenated functional groups such as carbonyls, carboxyls and ethers are formed during ozonolysis (Decesari et al., 2002; Kotzick et al., 1997). Although the formation of such functional groups could not be precisely identified through elemental analysis, thermogravimetry or FTIR spectroscopy, the combination of the results obtained through these different techniques suggests a production of oxygenated compounds. For example, *n*-hexane soot lost 27.1 % of its initial carbon mass during oxidation while more than doubling its oxygen content (+118 %, see Table 4 above), thus indicating formation of oxygenated functional groups and loss of carbon through production of small volatile organic molecules.

The labilization of *n*-hexane soot can also be observed in the thermograms of the natural and oxidized soot samples in the form of a shift in the peak lower temperature boundary to a lower temperature, suggesting important structural changes upon oxidation leading to a loss of thermal refractoriness. Figure 22 visibly identifies such change in the molecular structure of *n*-hexane soot as a fraction of the sample that was originally oxidized between 574 and 610 °C in the non-treated soot sample was shifted to lower temperatures after oxidation (mainly between 300 and 420 °C). The molecular changes observed in the thermograms possibly reflect a labilization of the soot component through the formation of hydrophilic groups such as carboxylic acids, esters, ketones and ethers (Smith & Chughtai, 1995; Stanmore et al., 2001). Formation of polar groups during oxidation of soot also favors adsorption of water onto the molecular structure of the BC component, as seen with the peak maximum at 200 °C most likely corresponding to a loss of water and small volatile organic molecules.

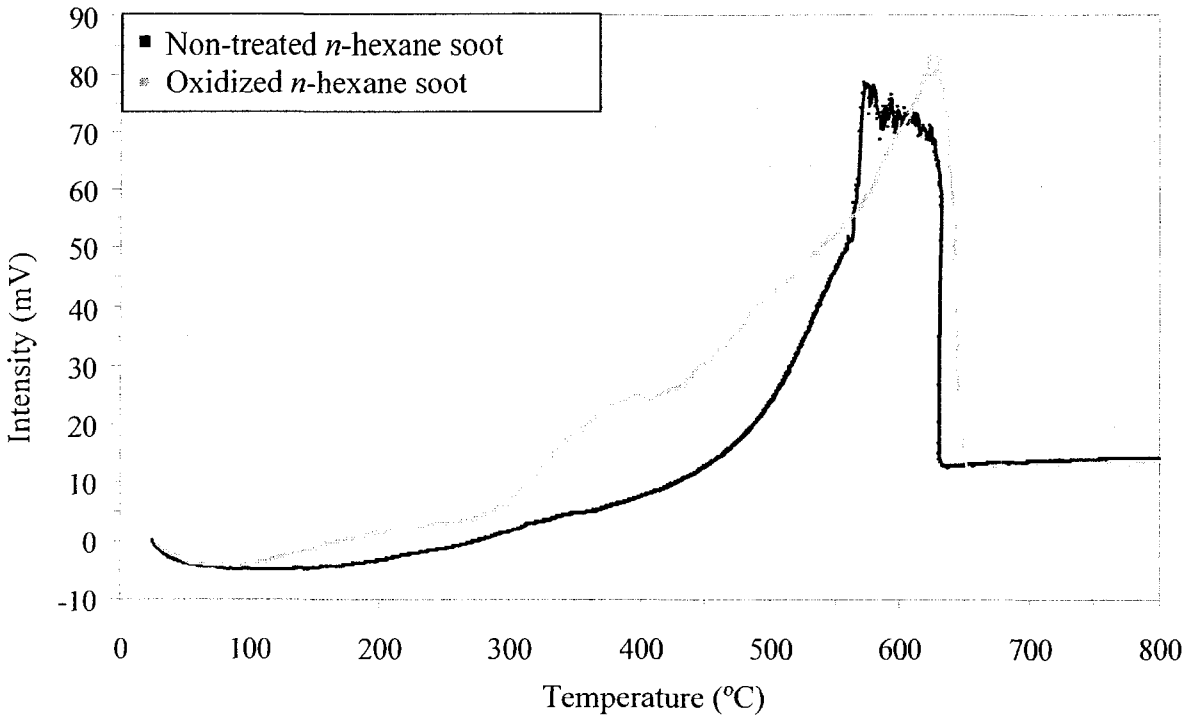

Figure 22. Changes in thermal resistance of *n*-hexane soot following oxidation

The formation of polar groups in *n*-hexane soot probably occurs through a different pathway than in graphite since its molecular structure contains more hydrophilic functional groups. Figure 23 is a functional representation of the *n*-hexane soot structure as proposed by Akther et al. (1985) and used since then by many others (Chughtai et al., 2003; Hammes, 2007; Masiello, 1998; Schmidt and Noak, 2000).

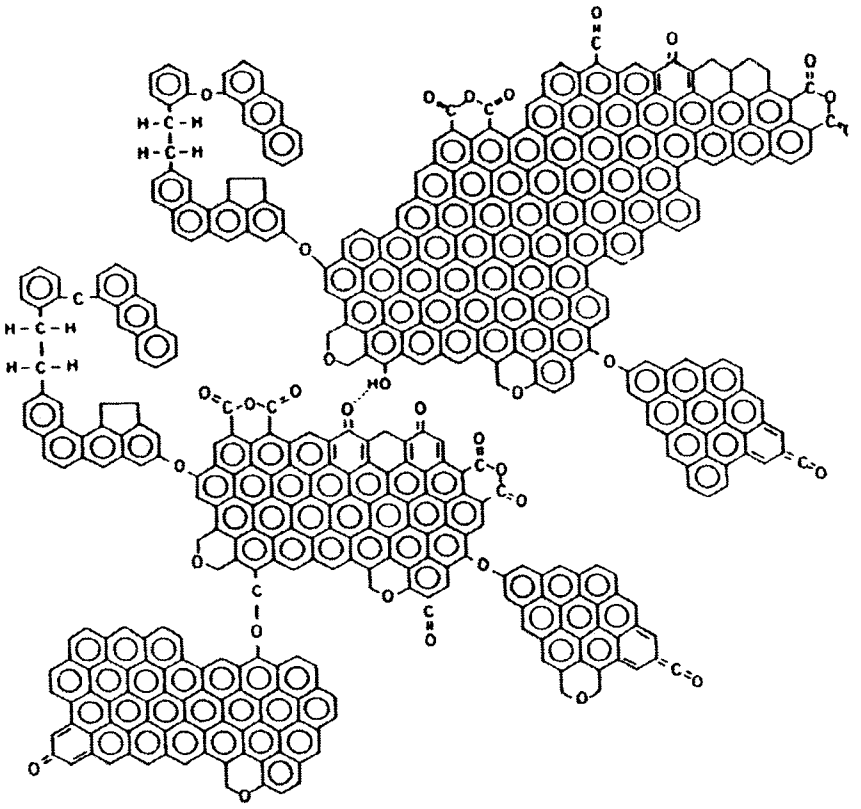

Figure 23. Molecular representation of *n*-hexane soot proposed by Akhter et al. (1985).

The greater lability of *n*-hexane soot suggests that the ozonolysis mechanism for this component is somewhat different than for graphite. The ozonolysis mechanism shown below (Figure 24) presents another possible pathway to the oxidation of *n*-hexane soot by UV radiation and ozone exposure. It is based on the Criegee mechanism in which an ozone molecule undergoes 1-3 dipolar cycloaddition with carbon double or triple bonds, forming a primary ozonide, also called molozonide, followed by the formation of a secondary ozonide. The molozonides can be converted into aldehydes or carboxylic acids in presence of water, by protonation of the intermediate product. A study of the oxidation of amorphous carbon by ozone under anhydrous conditions also

revealed that the formation of hydroxyl groups may result from the interactions with aliphatic species (Mawhinney & Yates, 2001).

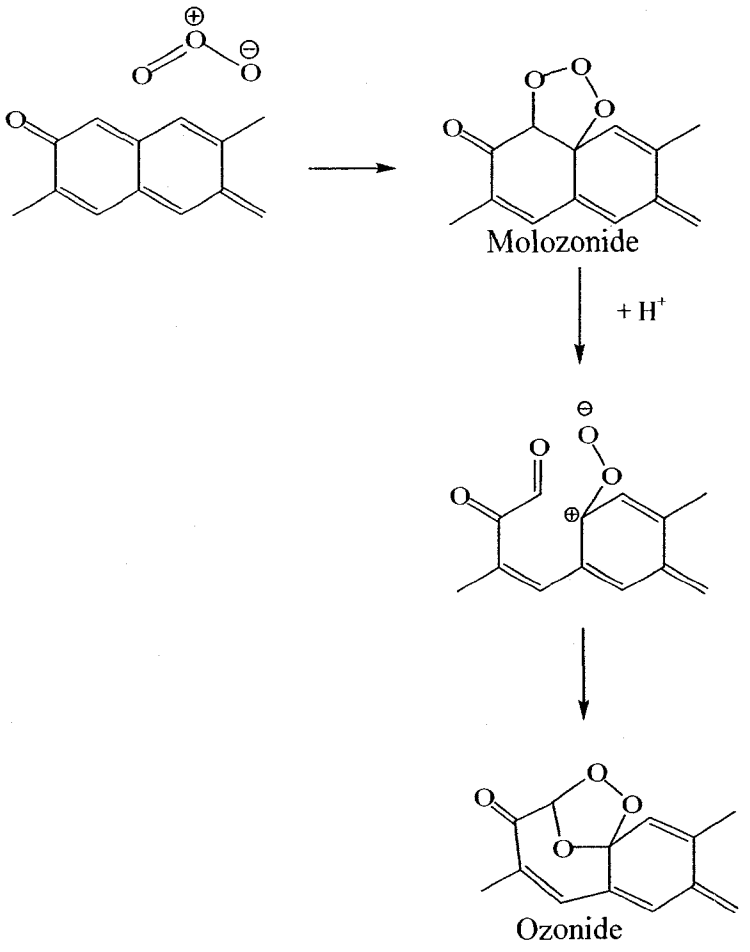

Figure 24. Ozonolysis mechanism of BC material as proposed by Mawhinney and Yates (2001).

Thermal methods can be of assistance in the determination of the thermal lability of the different BC components but they also have been used to differentiate between labile and refractory fractions of soil organic matter (Plante et al., 2005), in the classification of coal into ranks (Kok, 2002) and in the differentiation of pure BC components (Leifeld,

2007). The thermal oxidizability of non-treated and oxidized graphite, *n*-hexane soot, bituminous coal and an isolate of Stillaguamish River sediment were thus compared to assess changes in thermal stability likely indicative of changes in the molecular composition/structure of the components during oxidation, as well as to evaluate the possibility of exploiting thermogravimetry as an approach to separately quantify and/or isolate one or many BC components. Figure 25 shows that graphite can easily be distinguished from the other BC components, as it is thermally stable below a temperature of 642 °C, while soot and bituminous coal samples are completely oxidized. Soot and bituminous coal, however, cannot be separated from one another using this technique since the beginning of the DTA peak measured for bituminous coal falls right within the temperature range corresponding to the maximum of the peak detected for soot (~593 °C). Although it is often assumed that the chemical lability of a component is adequately reflected by its thermal oxidizability, the results obtained here suggest otherwise. Indeed, the stability of graphite and soot towards ozone oxidation reflects their thermal stabilities (with carbon losses through ozone exposure of 5.27 % and 27.1 %, respectively, and maximum differential thermogravimetric peaks of 838 °C and 593 °C, respectively). However, the loss of carbon mass for the bituminous coal sample (4.57 %) is not an indication of its thermal stability as the maximum of the DTA peak occurs at a lower temperature than those of graphite and soot (565 °C). This result provides another indication that thermogravimetric methods are not suitable to efficiently separate BC components based on their thermal stabilities. Thus, thermal stability most likely is not an adequate proxy to assess the environmental stability or resistance to chemical oxidation of BC compounds. The overlapping ranges of thermal stability obtained for *n*-

hexane soot and bituminous coal and thus, the inadequacy of DTA to quantitatively measure or separate these two BC components concur with published results assessing the potential of TG/DTA for the measurement of different BC material (Leifeld, 2007).

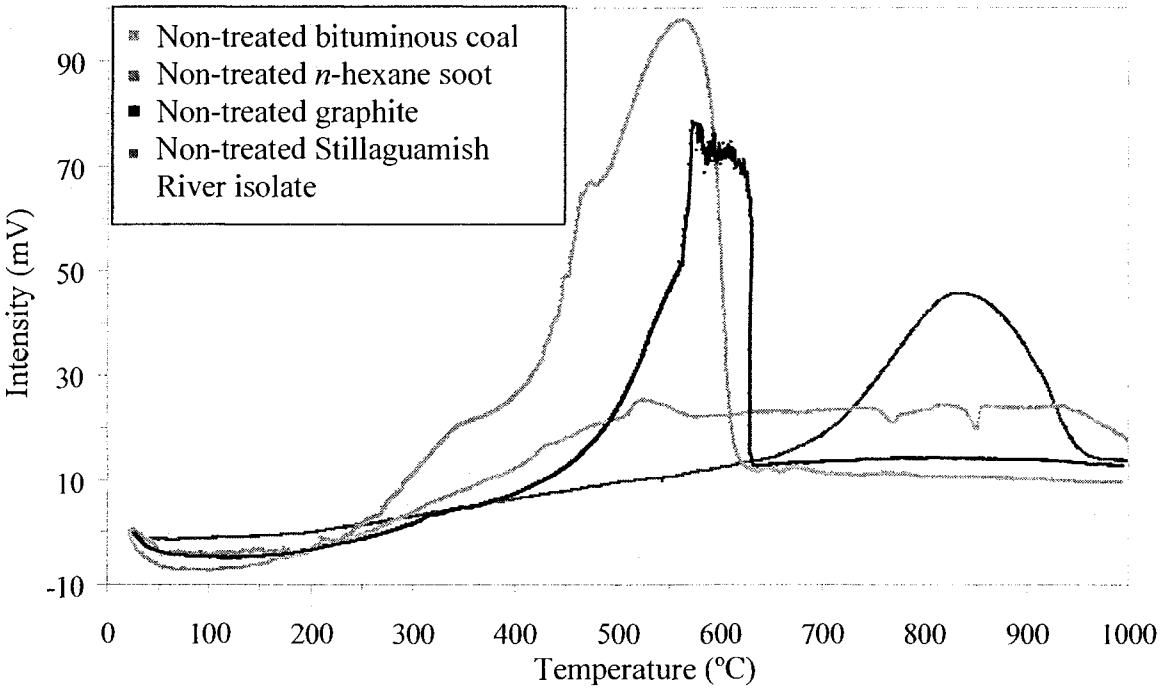

Figure 25. Changes in thermal resistance of bituminous coal, *n*-hexane soot, graphite and Stillaguamish River isolate before UV radiation and ozone oxidation. (Note that the *y*-axis for the Stillaguamish River isolate was multiplied by 2 to facilitate visual comparison with the other samples).

The DTA curve seen on Figure 25 also provides clues on the composition of the Stillaguamish River isolate. The presence of soot, or other related combustion derived materials, can be deduced from the exothermic peak between 413 °C and 583 °C. As explained in the *Methods* section, coal components are removed during the thermal

oxidation step of the isolation method for soot and graphitic carbon and therefore cannot be present in the isolate. The first mass derivative of the isolate, as seen on Figure 26, amplifies the signal for graphitic carbon in the isolate by presenting the changes in mass of the sample as a function of temperature.

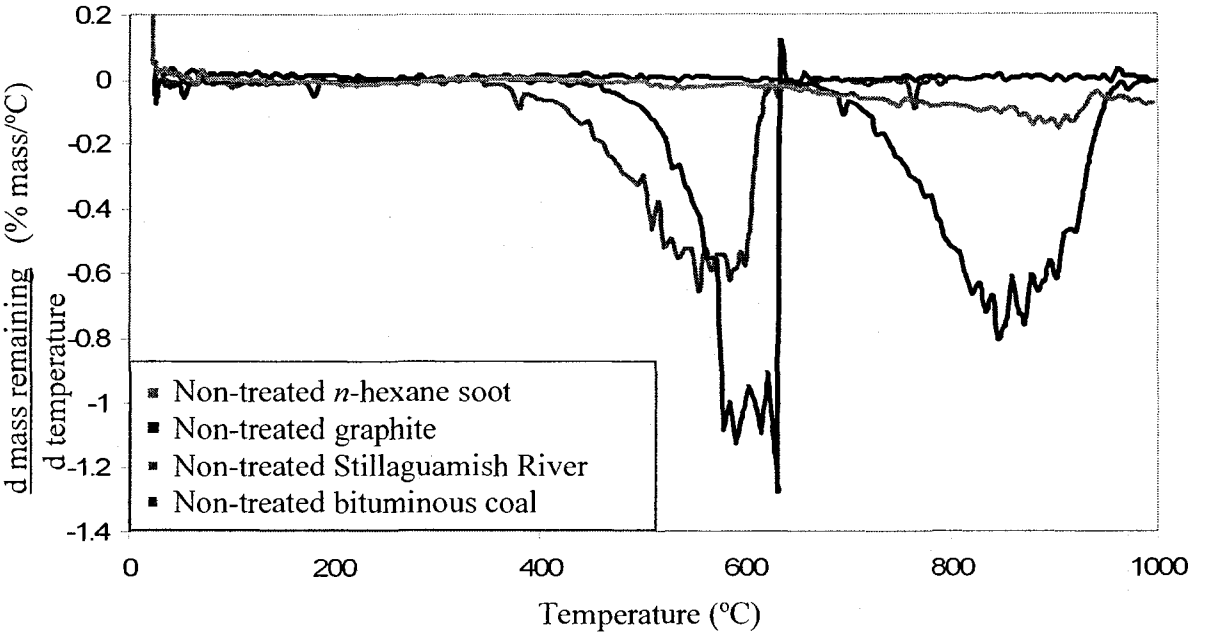

Figure 26. First mass derivatives of non-treated graphite, soot and Stillaguamish River isolate before UV radiations and ozone oxidation

The mass derivatives seen on Figure 26 also suggest that graphitic carbon seems to be present in greater concentration than soot in the Stillaguamish River isolate as its derivative peak height is approximately 1.6 times greater in the graphitic carbon region than the soot region. Since the mass derivative graph represents the rate of mass loss, a comparison of the slopes can give a good estimate of either the quantity or the size of molecules lost upon heating. As oxidation of soot and graphite are thought to occur

mainly through the loss of low molecular weight molecules, the slopes observed in the first derivative thermogram can be used as a comparison tool to qualitatively assess the loss of low-molecular weight molecules during a certain temperature period. The slopes of the isolate in the soot and graphitic carbon regions (-0.00022 and -0.00035 % mass remaining/°C, at 555 and 773 °C respectively) indicate a larger quantity of low-molecular weight molecules lost in the graphitic carbon region as compared to the soot region by approximately 1.6 times. Moreover, the graphitic carbon derivative peak is almost three times wider than that of soot, thus indicating a wider temperature range over which oxidation involving larger quantities of low-molecular weight molecules takes place. These results correlate with a recently published article on the composition of Stillaguamish River isolate obtained by X-ray spectromicroscopy in which approximately 80 % of the carbon is reported as graphitic carbon and 17 % as a more aliphatic form of carbon, possibly originating from soot-like structures (Haberstroh et al., 2006).

Oxidation of the isolate of Stillaguamish River is clearly demonstrated in the thermogram seen in Figure 27. In this thermogram, a large portion of the more refractory components thermally oxidized above 502 °C in the non-treated isolate is lost and replaced by more thermally labile material that oxidizes between 150 °C and 463 °C. The carbon loss upon oxidation of the isolate is further confirmed by EA with a 79 % reduction in carbon mass (from 2.7 mg to 0.6 mg). Changes in oxygen content of the sample could not be monitored owing to the presence of oxygen-containing minerals in the isolate. However, the formation of a new exothermic peak at about 65 °C is

indicative of water adsorption and therefore suggests the formation of polar groups upon oxidation.

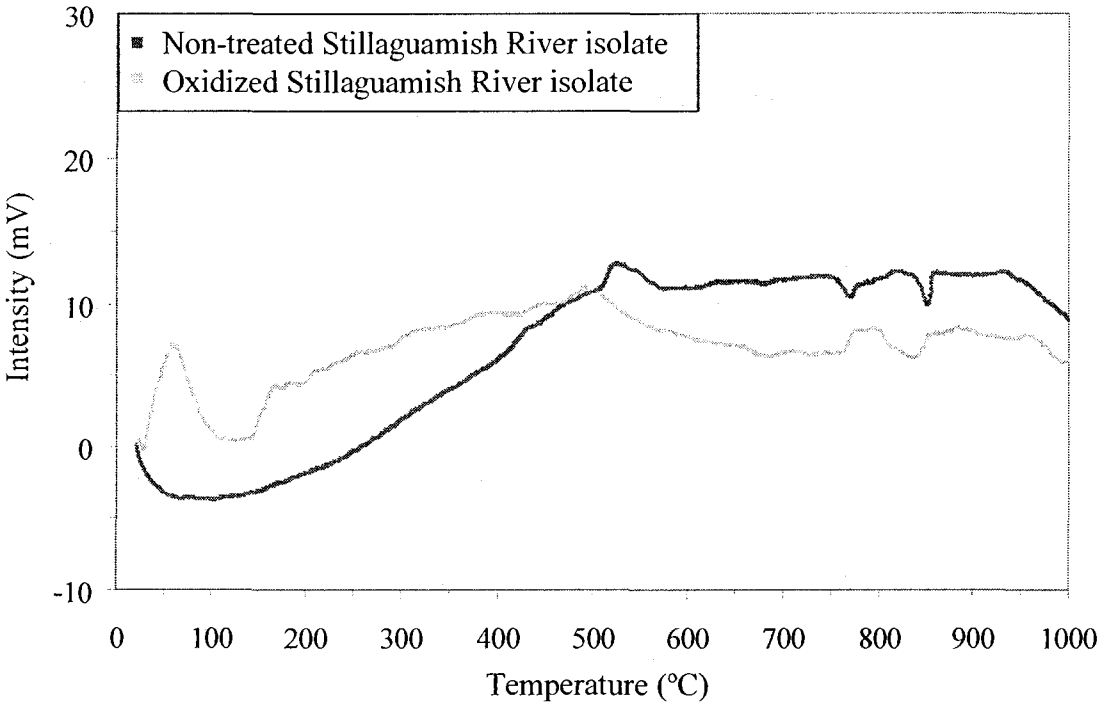

Figure 27. Changes in thermal resistance of Stillaguamish River isolate soot following oxidation

The thermogravimetric traces obtained for the isolate of Stillaguamish River suggest the presence of a large proportion of graphitic carbon in the natural isolate. Again, this result agrees with the report of Haberstroh et al. (2006) in which graphite was identified as a major component of the isolate. The results also agree with the heavy-liquid fractionation results obtained on the same isolate (7.6 % soot and 92.4 % graphitic carbon).

Oxidation of bituminous coal, *n*-hexane soot, graphite and a natural isolate of Stillaguamish River through exposure to UV radiations and ozone was observed through changes in the elemental composition and thermal oxidizability of the compounds. Most of the elemental results agree with the reported thermal lability of the compounds with, for example, large carbon mass losses of 27.1, 36 and 34.2 % for *n*-hexane soot, urban atmospheric particulate and melanoidin, respectively, and a much lower loss for refractory graphite (5.27 % C). On the other hand, bituminous coal, a BC compound more thermally labile than graphite, lost a lot less carbon than expected with a reduction of only 4.6 % in carbon mass. This surprising result may be explained by the obstruction of the internal pores of the bituminous coal with newly formed oxygenated functional groups, or because of partial oxidation that may have occurred prior to the study. As a result, the photochemical oxidizability of a component might not reflect its thermal oxidizability, as often assumed, since the rate of oxidation of bituminous coal was lower than expected.

The oxidizability of a natural isolate of the Stillaguamish River resulted in a carbon loss of 79 %, suggesting that the soot and graphitic carbon isolate of natural samples might not be as refractory as commonly assumed. Its soot and graphitic carbon composition was also assessed from thermogravimetry. Although this technique is not quantitative, the thermograms obtained clearly indicate a greater relative abundance of graphitic carbon compared to soot in the isolate. This result is in agreement with results recently obtained from the same isolate (Haberstroh et al. 2006). The differentiation and separation potential of DTA for different BC components were also determined to be

inefficient for bituminous coal and *n*-hexane soot since these two compounds have very similar maximum DTA peaks with values of median temperature values of 565 and 593 °C, respectively.

While the photolysis and ozonolysis experiment demonstrated that oxidation of compounds as refractory as graphite leads to a decrease in the relative abundance of highly recalcitrant carbon components and a concomitant increase of more thermally labile and sometimes volatile organic matter, the impact of these changes on the global carbon cycle remains to be studied.

5. Conclusion and future work

The global carbon cycle is composed of many biogeochemical processes including the geological carbon cycle, which, through metamorphism, produces graphitic carbon. This graphitic carbon is highly stable chemically because of its macromolecular and compact structure and thus was assumed to be virtually impossible to degradation under normal environmental conditions. This characteristic suggests that graphitic carbon, unlike other less refractory BC components, continuously cycles almost quantitatively between the crust and the surface of the Earth, with little chemical alterations. Since graphitic carbon is not as refractory as commonly assumed, the implications of the addition of low-molecular weight and sometimes volatile organic compounds to the atmosphere will have to be evaluated in order to better constrain the slowly-cycling component of the global carbon cycle. To do that, and to shed light on the oxidation reaction pathways and rates, better characterization tools and approaches will have to be developed, paralleled by efforts to increase the precision and accuracy of elemental analysis of thermally refractory, high carbon and low oxygen containing components.

Until new analytical approaches are developed, some characteristics of BC compounds should be investigated to better understand their oxidation pathways and hence their role in the global carbon cycle. First, the link between porosity of a compound and its lability towards oxidation should be probed. As observed in this project, bituminous coal did not exhibit the same susceptibility towards chemical oxidation as generally assumed. One of the possible reason for this unexpected behaviour is a high porosity, as explained in Chapter 4. Since coal particles are characterized by

pores that vary over a very wide range of sizes, it would be of interest to evaluate the relationship between pore size and the type of functional groups present on a compound, in relation with the sample susceptibility to oxidation. Such a study could be carried out using X-ray spectromicroscopy, a technique that can be used to identify functional groups and determine their location at the sub-micrometer scale at the surface of a sample (Haberstroh et al., 2005). Another important aspect would be to study the effect of aging (and thus modification of surface functional groups) on the chemical and thermal lability of BC compounds. Upon aging, charged functional groups may form on the otherwise hydrophobic surface of polyaromatic materials and thus, change the properties of BC compounds. Such groups could for instance limit the accessibility of oxidants by blocking the opening of small pores, resulting in a decrease in their lability compared to their non-altered counterpart, as explained above and in Chapter 4 for the bituminous coal sample used in this work. They could also enhance their oxidation rate through catalytic reactions following the complexation of reaction metal species on the "activated" surface. Despite our work and that of several other research teams, our chemical understanding of the reactions that control the fate of BC compounds in the environment is still in its infancy.

Another element of importance to improve our comprehension of the role of BC compounds in the global carbon cycle is the ability to separate and study the soot and graphitic carbon phases independently. Although the heavy-liquid fractionation technique developed in this project allows for such separation, the absolute efficiency of the separation (recovery of soot and graphitic carbon in their respective isolates) could

not be assessed accurately and precisely using the stable carbon isotope signatures of the two pure phases simply because they were very close. The use of another source of soot, such as soot produced during the combustion of highly depleted C4-type plant tissues (grasses and bushes), could remediate this problem. A difference of about 10 ‰ between the signatures of soot and graphite (as opposed to about 1 ‰ in this work) would have increased accuracy and precision by about one order of magnitude, thus allowing to conclude with a sufficiently high level of confidence whether the fractionation of soot and graphite was successful.

The work presented in this thesis sums up one of the first studies on the reactivity of BC compounds in the environment, and the very first one looking specifically at the reactions influencing the cycle of the most refractory components of the BC continuum. Because of the difficulties associated with the analysis of polyaromatic, condensed materials, the focus of further research should be placed on the optimization of novel methods that allow characterizing the structure and chemical composition of pure BC standards as well as isolates of altered soot and graphitic carbon. Given the continued development and innovation in analytical organic geochemistry, great advances in our comprehension of the slowly cycling carbon pools are expected in the next decade.

5.1 References

Akhter, M. S., Chughtai, A. R. & Smith, D. M. (1985). The structure of hexane soot I: Spectroscopic studies. *Applied Spectroscopy*, **39**(1), 143-153.

Allard, B., Templier, J. & Largeau, C. (1998). An improved method for the isolation of artifact-free algaenans from microalgae. *Organic Geochemistry*, **28**(9-10), 543-548.

Apatiga, L. M., Castaneda-Miranda, A., Menchaca, C. & Castano, V. M. (2002). Selective oxidation of graphite on diamond films induced by UV exposure. *Inorganic Materials*, **38**(1), 31-33.

Backreedy, R., Jones, J. M., Pourkashanian, M. P. & Williams, A. (2001). A study of the reaction of oxygen with graphite : Model chemistry. *Faraday Discussions*, **119**, 385-394.

Berner, R. A. (2003). The long-term carbon cycle, fossil fuels and atmospheric composition. *Nature*, **426**(6964), 323-326.

Bond, T. C. & Bergstrom, R. W. (2006). Light absorption by carbonaceous particles: An investigative review. *Aerosol Science & Technology*, **40**(1), 1-41.

Braun, T., Osawa, E., Detre, C. & Toth, I. (2001). On some analytical aspects of the determination of fullerenes in samples from the permian/triassic boundary layers. *Chemical Physics Letters*, **348**, 361-362.

Burdige, D. J. (2007). Preservation of organic matter in marine sediments: Controls, mechanisms, and an imbalance in sediment organic carbon budgets? *Chemical Reviews*, **107**(2), 467-485.

Cachier, H., Liousse, C., Buatmenard, P. & Gaudichet, A. (1995). Particulate content of savanna fire emissions. *Journal of Atmospheric Chemistry*, **22**(1-2), 123-148.

Choi, M. Y., Mulholland, G. W., Hamins, A. & Kashiwagi, T. (1995). Comparisons of the soot volume fraction using gravimetric and light extinction techniques. *Combustion and Flame*, **102**(1-2), 161-169.

Chughtai, A. R., Kim, J. M. & Smith, D. M. (2003). The effect of temperature and Humidity on the reaction of ozone with combustion soot: Implications for reactivity near the Tropopause. *Journal of Atmospheric Chemistry*, (45) 231-243

Ciais, P., Dennings, A. S., Tans, P. P., Berry, J. A., Randall, D. A., Collatz, G. J., Sellers, P. J., White, J. W. C., Trolier, M., Meijer, H. A. J., Francey, R. J., Monfray, P. & Heimann, M. (1997). A three-dimensional synthesis study of $\delta^{18}O$ in atmospheric CO_2 1. Surface fluxes. *Journal of Geophysical Research*, **102**(D5), 5857-5872.

Clark, I. D. & Fritz, P. (1997). *Environmental isotopes in hydrogeology*. Lewis Publishers, New York.

Cornelissen, G. & Gustafsson, O. (2005). Prediction of large variation in biota to sediment accumulation factors due to concentration-dependent black carbon adsorption of planar hydrophobic organic compounds. *Environmental Toxicology and Chemistry*, **24**(3), 495-498.

Daniels, E. J., Aronson, J. L., Altaner, S. P. & Clauer, N. (1994). Late Permian age of NH_4-bearing illite in anthracite from Eastern Pennsylvanian-temporal limits on coalification in the Central Appalachians. *Geological Society of America Bulletin*, **7**, 760-766.

Decesari, S., Facchini, M. C., Matta, E., Mircea, M., Fuzzi, S., Chughtai, A. R. & Smith, D. M. (2002). Water soluble organic compounds formed by oxidation of soot. *Atmospheric Environment*, **36**(11), 1827-1832.

Dickens, A. F., Gélinas, Y. & Hedges, J. I. (2004). Physical separation of combustion and rock sources of graphitic black carbon in sediments. *Marine Chemistry*, **92**(1-4), 215-223.

Druffel, E. R. M. (2004). Comments on the importance of black carbon in the global carbon cycle. *Marine Chemistry. New Approaches in Marine Organic Biogeochemistry: A Tribute to the Life and Science of John I. Hedges*, **92**(1-4), 197-200.

Elmquist, M., Gustafsson, O. & Andersson, P. (2004). Quantification of sedimentary black carbon using the chemothermal oxidation method: and evaluation of ex situ pretreatments and standard additions approaches. *Limnology and Oceanography: Methods 2*, 417-427.

Fernandes, M. B. & Brooks, P. (2003). Characterization of carbonaceous combustion residues: II. Nonpolar organic compounds. *Chemosphere*, **53**, 447-458.

Fernandes, M. B., Skjemstad, J. O., Johnson, B. B., Wells, J. D. & Brooks, P. (2003). Characterization of carbonaceous combustion residues. I. Morphological, elemental and spectroscopic features. *Chemosphere*, **51**, 785-795.

Forbes, M. S., Raison, R. J. & Skjemstad, J. O. (2006). Formation, transformation and transport of black carbon (charcoal) in terrestrial and aquatic ecosystems. *Science of the Total Environment*, **370**(1), 190-206.

Francis, W. (1954). *Coal. Its formation and composition.* Edward Arnold Ltd, London.

Garrels, R. M., Lerman, A. & Mackenzie, F. T. (1976). Controls of atmospheric O_2 and CO_2 - past, present, and future. *American Scientist*, **64**, 306-315.

Gélinas, Y., Prentice, K. M., Hedges, J. I. & Baldock, J. A. (2001). An improved thermal oxidation method for the quantification of soot/graphitic black carbon in sediments and soils. *Environmental Science & Technology*, **35**(17), 3519-3525.

Glaser, B., Lehmann, J. & Zech, W. (2002). Ameliorating physical and chemical properties of highly weathered soils in the tropics with charcoal - a review. *Biology and Fertility of Soils*, **35**(4), 219-230.

Goni, M. A., Yunker, M. B., Macdonald, R. W. & Eglinton, T. I. (2005). The supply and preservation of ancient and modern components of organic carbon in the Canadian Beaufort Shelf of the Arctic Ocean. *Marine Chemistry*, **93**(1), 53-73.

Griffin, J. J. & Goldberg, E. D. (1975). The fluxes of elemental carbon in coastal marine sediments *Limnology and Oceanography*, **20**, 456-463.

Gustafsson, O. & Gschwend, P. M. (1998). The flux of black carbon to surface sediments on the New England continental shelf *Geochimica et Cosmochimica Acta*, **62**, 465-472.

Haberstroh, P. R., Brandes, J. A., Gélinas, Y., Dickens, A. F., Wirick, S. & Cody, G. D. (2006). Chemical composition of the graphitic black carbon fraction in riverine and marine sediments at sub-micron scales using carbon X-ray spectromicroscopy. *Geochimica et Cosmochimica Acta*, **70**(6), 1483-1494.

Hahn, J. R. (2005). Kinetic study of graphite oxidation along two lattice directions. *Carbon*, **43**(7), 1506-1511.

Hammes, K., et al. (2007). Comparison of quantification methods to measure fire-derived (black-elemental) carbon in soils and sediments using reference materials from soil, water, sediment and the atmosphere. *Global Biogeochemical Cycles*, **21**. GB3016

Hedges, J. I. & Keil, R. G. (1995). Sedimentary organic-matter preservation - an assessment and speculative synthesis. *Marine Chemistry*, **49**(2-3), 81-115.

Hedges, J. I., Keil, R. G. & Benner, R. (1997). What happens to terrestrial organic matter in the ocean? *Organic Geochemistry*, **27**(5/6), 195-212.

Holland, H. D. (1978). *The Chemistry of the Atmosphere and Oceans*. Wiley-Interscience, New York.

Houghton, R. A. (2003). The Contemporary carbon cycle. 1 ed. In *Treatise on Geochemistry*, ed. H. D. H. a. K. K. Turekian, Vol. 8, Elsevier-Pergamon. Oxford, U. K., pp. 473-513.

Kennedy, I. M. (1997). Models of soot formation and oxidation. *Progress in Energy and Combustion Science*, **23**(2), 95-132.

Kim, W.-S., Park, Y. H., Shin, J. Y., Lee, D. W. & Lee, S. (1999). Size determination of diesel soot articles using flow and sedimentation field-flow fractionation. *Analytical Chemistry*, **71**(15), 3265-3272.

Kok, M. V. (2002). Thermal analysis applications in fossil fuel science. *Journal of Thermal Analysis and Calorimetry*, **68**, 1061-1077.

Kotzick, R., Panne, U. & Niessner, R. (1997). Changes in condensation properties of ultrafine carbon particles subjected to oxidation by ozone. *Journal of Aerosol Science*, **28**(5), 725-735.

Krishnaswamy, S., Gunn, R. D. & Agarwal, P. K. (1996). Low-temperature oxidation of coal. 2. An experimental and modelling investigation using a fixed-bed isothermal flow reactor. *Fuel*, **75**(3), 344-352.

Kuhlbusch, T. A. J. & Crutzen, P. J. (1995). Toward a global estimate of black carbon in residues of vegetation fires representing a sink of atmospheric CO_2 and a source of O_2. *Global Biogeochemical Cycles*, **9**(4), 491-501.

Kwiecinska, B. & Petersen, H. I. (2004). Graphite, semi-graphite, natural coke, and natural char classification--ICCP system. *International Journal of Coal Geology*, **57**(2), 99-116.

Langley, L. A., Villanueva, D. E. & Fairbrother, D. H. (2006). Quantification of surface oxides on carbonaceous materials. *Chemistry of Materials*, **18**(1), 169-178.

Leifeld, J. (2007). Thermal stability of black carbon characterised by oxidative differential scanning calorimetry. *Organic Geochemistry*, **38**, 112-127.

Lerf, A., He, H. Y., Forster, M. & Klinowski, J. (1998). Structure of graphite oxide revisited. *Journal of Physical Chemistry B*, **102**(23), 4477-4482.

Li, J.-L., Kudin, K. N., McAllister, M. J., Prud'homme, R. K., Aksay, I. A. & Car, R. (2006). Oxygen-driven unzipping of graphitic materials. *Physical Review Letters*, **96**(176101), 1-4.

Li, Y.-H. (2000). A compendium of geochemistry. In *Princeton University Press*, Vol. xiv, pp. 300.

Lloyd, J. & Farquhar, G. D. (1996). The CO_2 dependence of photosynthesis, plant growth responses to elevated atmospheric CO_2 concentrations, and their interection with

soil nutrient status. I. General principles and forest ecosystems. *Functional Ecology*, **10**, 4-32.

Mackenzie, F. T., Lerman, A. & Andersson, A. J. (2004). Past and present of sediment and carbon biogeochemical cycling models. *Biogeosciences*, **1**(1), 11-32.

Maillard, L. C. (1912). Action des acides aminés sur les sucres: formation des mélanoidines par voie méthodologique. *Comptes Rendus de l'Academie des Sciences (Paris)*, **156**, 148-149.

Masiello, C. A. & Druffel, E. R. M. (1998). Black carbon in deep-sea sediments *Science*, **280**, 1911-1913.

Masiello, C. A. (2004). New directions in black carbon organic geochemistry. *Marine Chemistry*, **92**(1-4), 201-213.

Mawhinney, D. B. & Yates, J. T. (2001). FTIR study of the oxidation of amorphous carbon by ozone at 300 K - Direct COOH formation. *Carbon*, **39**(8), 1167-1173.

Nunes, F. M. & Coimbra, M. A. (2007). Melanoidins from coffee infusions. Fractionation, chemical characterization, and effect of the degree of roast. *Journal of Agriculture and Food Chemistry*, **55**, 3967-3977.

Ogren, J. A. & Charlson, R. J. (1983). Elemental carbon in the atmosphere: cycle and lifetime. *Tellus*, **35B**, 241– 254.

Orem, W. H. & Finkelman, R. B. (2003). Coal formation and geochemistry. 1 ed. In *Treatise on Geochemistry*, ed. H. D. H. a. K. K. Turekian, Vol. 7, Elsevier-Pergamon. Oxford, U. K., pp. 191-222.

Patrakov, Y. F., Fedyaeva, O. N., Semenova, S. A., Fedorova, N. I. & Gorbunova, L. V. (2006). Influence of ozone treatment on change of structural-chemical parameters

of coal vitrinites and their reactivity during the thermal liquefaction process. *Fuel*, **85**(9), 1264-1272.

Pierson, H. O. (1993). *The handbook of carbon, graphite, diamond and fullerene: properties, processing and applications*. Noyes Publications, Park Ridge.

Penner, J. E., Eddleman, H. & Novakov, T. (1993). Towards the development of a global inventory for black carbon emissions. *Atmospheric Environment. Part A. General Topics*, **27**(8), 1277-1295.

Pesek, J. & Sykorova, I. (2006). A review of the timing of coalification in the light of coal seam erosion, clastic dykes and coal clasts. *International Journal of Coal Geology*, **66**(1-2), 13-34.

Plante, A. F., Pernes, M. & Chenu, C. (2005). Changes in clay-associated organic matter quality in a C depletion sequence as measured by differential thermal analyses. *Geoderma*, **129**(3-4), 186-199.

Prentice, L. C., Farquhar, G. D., Fasham, M. J. R., Goulden, M. L., Heimann, M., Jaramillo, V. J., Kheshgi, H. S., Quere, C. L., Scholes, R. J. & Wallace, D. W. R. (2001). The carbon cycle and atmospheric carbon dioxide. In *Climate Change 2001: The Scientific Basis. Contribution of Working Group I to the Third Assessment Report of the Intergovernmental Panel on Climate Change*, eds. J. T. Houghton, Y. Ding, D. J. Griggs, M. Noguer, P. J. van der Linden, X. Dai, K. Maskell & C. A. Johnson, Cambridge University Press. Cambridge, United Kingdom, New York, NY, USA.

Sanchez, A. & Mondragon, F. (2007). Role of the epoxy group in the heterogeneous CO_2 evolution in carbon oxidation reactions. *Journal of Physical Chemistry C*, **111**(2), 612-617.

Sarmiento, J. L. (1993). Ocean carbon cycle. *Chemical & Engineering News*, **71**, 30-43.

Schlunz, B. & Schneider, R. R. (2000). Transport of terrestrial organic carbon to the oceans by rivers: re-estimating flux- and burial rates. *International Journal of Earth Sciences*, **88**(4), 599-606.

Schmidt, M. W. I. & Noack, A. G. (2000). Black carbon in soils and sediments: Analysis, distribution, implications, and current challenges. *Global Biogeochemical Cycles*. **14**(3), 777-793.

Schmidt, M. W. I., Skjemstad, J. O., Czimczik, C. I., Glaser, B., Prentice, K. M., Gélinas, Y. & Kuhlbusch, T. A. J. (2001). Comparative analysis of black carbon in soils. *Global Biogeochemical Cycles*, **15**(1), 163-167.

Smith, D. M. & Chughtai, A. R. (1995). The surface structure and reactivity of black carbon. *Colloids and Surfaces A: Physicochemical and Engineering Aspects*, **105**(1), 47-77.

Stanmore, B. R., Brilhac, J. F. & Gilot, P. (2001). The oxidation of soot: a review of experiments, mechanisms and models. *Carbon*, **39**(15), 2247-2268.

Suchet, P. A., Probst, J.-L. & Ludwig, W. (2003). Worldwide distribution of continental rock lithology: Implications for the atmospheric/soil CO_2 uptake by continental weathering and alkalinity river transport to the oceans. *Global Biogeochemical Cycles*, **17**(2), 1038.

Sundquist, E. T. & Visser, K. (2004). The geologic history of the carbon cycle. First ed. In *Treatise on Geochemistry*, ed. H. D. Holland, Turekian, K. K., Vol. 8, Elsevier-Pergamon. Oxford, pp. 425-472.

Swann, P. D. & Evans, D. G. (1979). Low-temperature oxidation of brown coal. 3. Reaction with molecular oxygen at temperatures close to ambient. *Fuel*, **58**, 276-280.

Taylor, G. H., Teichmfller, M., Davis, A., Diessel, C. F. K., Littke, R. & Robert, P. (1998). *Organic Petrology*. Gebrfder Borntraeger, Berlin.

Verardo, D. J. (1997). Charcoal analysis in marine sediments *Limnolology and Oceanography*, **42**, 192-197.

Wang, H., Dlugogorski, B. Z. & Kennedy, E. M. (2003). Coal oxidation at low temperatures: Oxygen consumption, oxidation products, reaction mechanism and kinetic modelling. *Progress in Energy and Combustion Science*, **29**(6), 487-513.

Waring, R. H., Landsberg, J. J. & Williams, M. (1998). Net primary production of forests: A constant fraction of gross primary production? *Tree Physiology*, **18**, 129-134.

Wood, B. J., Pawley, A. & Frost, D. R. (1996). Water and carbon in the Earth's mantle. *Philosophical Transactions of the Royal Society of A: Mathematical, Physical and Engineering Sciences*, **354**(1711), 1495-1511.

Zhu, H., Zhang, C., Tang, Y., Wang, J., Ren, B. & Yin, Y. (2007). Preparation and thermal conductivity of suspensions of graphite nanoparticles. *Carbon*, **45**(1), 226-228.

Zuberi, B., Johnson, K. S., Aleks, G. K., Molina, L. T. & Molina, M. J. (2005). Hydrophilic properties of aged soot. *Geophysical Research Letters*, **32**, 1-4.

Abbreviations

BC: Black carbon

DTA: Differential thermal analyzer

EA: Elemental analyzer

EA-IRMS: Elemental analyzer – Isotopic-ratio monitoring mass spectrometer

FTIR: Fourier-transform infrared

OC: Organic carbon

Glossary

Abrasion: Mechanical wearing of rock surfaces caused by inter-collisions.

Albite: A mineral found in granite rocks formed during low-temperature metamorphism.

Aerobic: A process involving oxygen.

Anaerobic: A process occurring in absence of oxygen.

Biological pump: A biogeochemical process involving the fixation of atmospheric carbon dioxide in the surface ocean.

Biosphere: Part of the world in which life exists

Black carbon. Material composed mainly of carbon and produced either by metamorphosis or as a by-product of fossil fuel or biomass combustion.

Coal: The product of stratified plant remains

Graphite: The most refractory black carbon compound. Produced from metamorphism.

Metamorphic processes: Chemical and crystallographic changes occurring in rocks present in the mantle of the Earth due to heat and pressure.

Orogeny: process by which mountain structures develop from the uplifting of tectonic plates

Photic zone: Water depth in an ocean or lake where photosynthesis occurs.

Phytoplankton: Drifting plant, animal, arechea or bacteria that live in the shallow water of the ocean.

Remineralization: Transformation of organic molecules into inorganic molecules.

Uplift: Movement of the Earth bending the Earth's crust..

Slaking: Physical breakdown of rocks caused by alternate wetting and drying cycles that increase the tensional stress of the rock due to the accumulation of successive water layers.

Solubility pump: Transport of carbon from the surface of the ocean to intermediate and deep waters.

Subduction: Process by which one tectonic plate descends beneath another.

Thermal insolation: Physical breakdown of rocks due to their expansion and contraction during diurnal temperature changes.

Weathering: Decomposition of rocks and minerals through contact with water, ice, heat and pressure.